2019

Hydrodynamic Limitations and the Effects of Living Shoreline Stabilization on Mangrove Recruitment along Florida Coastlines

Christian Pilato
University of Central Florida

HYDRODYNAMIC LIMITATIONS AND THE EFFECTS OF LIVING SHORELINE STABILIZATION ON MANGROVE RECRUITMENT ALONG FLORIDA COASTLINES

by

CHRISTIAN PILATO
B.S. University of Central Florida, 2016

A thesis submitted in partial fulfillment of the requirements
for the degree of Master of Science
in the Department of Biology
in the College of Sciences
at the University of Central Florida
Orlando, Florida

Spring Term

2019

Major Professor: Linda Walters

ABSTRACT

The recruitment success of mangroves is influenced by a variety of factors, including propagule availability, desiccation, herbivory, and hydraulic habitat limitations. Hydrodynamic forces (waves and currents) act as obstacles to mangrove recruitment, restricting the successful colonization of mangrove species. We evaluated the biological and physical limitations to mangrove recruitment through monthly shoreline surveys and lateral pull-tests. Surveys followed mangroves from propagule release through recruitment along the shorelines of De Soto National Memorial (Bradenton, FL), capturing differences in propagule availability and recruitment along natural areas and across differing forms of shoreline stabilization ("living shorelines" and revetments). Propagule densities were highest along "living shorelines", followed by natural areas and revetments. Seedling densities were similar across treatments, mirroring densities found in disturbed mangrove systems in the Philippines (<1 seedling per m^2). Pull-tests, simulating wave forces, quantified the physical thresholds for uprooting *Rhizophora mangle* and *Avicennia germinans* seedlings in both the greenhouse and field. Uprooting susceptibility significantly decreased with increased seedling biomass and age. *A. germinans* displayed a lower force to removal than *R. mangle*, but showed a greater increase in uprooting force with increases in size. Surrounding vegetation and canopy cover were not found to significantly affect the uprooting force of either species. Pull-test results were used in conjunction with drag coefficients from the literature to calculate flow velocities where mangroves would become susceptible to dislodgement from hydrodynamic forces. Seedlings tested would become susceptible at velocities of 7.33 ± 2.07 m/s for *A. germinans* and 5.40 ± 1.59 m/s for *R. mangle*. The rapid increase in force to removal shows the importance of disturbances, such as erosion, driving

seedling dislodgment at the local scale. This research strengthens our understanding of the physical conditions conducive to successful recruitment under hydrodynamic stressors and provides insight into how a common restoration method can influence mangrove recruitment.

ACKNOWLEDGEMENTS

Thank you to Dr. Linda Walters, Pedro F. Quintana-Ascencio, and Dr. Kelly Kibler for the help and guidance over the course of this project. Thank you to Melinda Donnelly, Suzanne Connor, Michelle Shaffer, Paul Sacks, and all members of the Coastal and Estuarine Ecology lab for the continued help with fieldwork and data collection. Thank you to the National Park Service for funding this project and the park staff at De Soto National Memorial and Canaveral National Seashore for help and cooperation throughout this work.

TABLE OF CONTENTS

LIST OF FIGURES

LIST OF TABLES

CHAPTER 1: INTRODUCTION

Mangroves are specialized woody plants that grow globally in saline to brackish water along the coastlines of the tropics and subtropics (Kathiresan and Qasim, 2005). Mangroves provide a variety of ecosystem services including erosion control, storm protection, raw materials, carbon sequestration, and act as a nursery habitat for a variety of ecologically and economically important fauna (e.g., Alongi, 2009; Barbier et al., 2011). Despite their intrinsic and economic importance, a substantial decline in global mangrove cover has been observed, with an overall ~35% reduction in habitat size since the 1980s (Polidoro et al., 2010; Giri et al., 2011; FAO, 2007). This decline has been attributed to a variety of anthropogenic stressors including coastal development, aquaculture expansion, and changes in hydrology (FAO, 2007; Barbier et al., 2011).

Mangroves inhabit mechanically challenging environments characterized by biophysical interactions and restrictions (Friess et al., 2012; Krauss et al., 2008). Their exposure on coastlines and lagoon edges leave them open to a variety of physical stressors, ranging from tropical storm force winds and waves to routine, low energy waves in more gentle lagoon environments (Kathiresan and Qasim, 2005; Alongi, 2009). In addition to mechanical challenges, mangroves are under ecophysiological stressors as well, such as variations in salinity (Ball, 1988) and temperature (Odum et al., 1982).

Mature mangrove communities are mechanically robust and able to withstand and dissipate routine local wave energy (e.g. Alongi, 2009; Mazda et al., 2005; Mazda et al., 1997). However, focused research on early life-stages in the field is needed as there remains a distinct gap in the literature regarding the influence of these hydrodynamic forces on propagule

establishment. Recruitment and mangrove establishment occurs when mangrove propagules end their free-floating dispersal phase by rooting into the substrate, entering the seedling phase. During the seedling phase, seedlings are single stemmed and flexible (Boizard and Mitchell, 2011). While this phase is characterized by rapid root and stem growth, the initial size makes the seedling phase particularly vulnerable to physical stressors (Lima et al., 2018). As seedlings transition to juveniles, stem thickening, secondary branching, and the development of more complex root structures begin (e.g. prop roots, pneumatophores) (Boizard and Mitchell, 2011). These initial stages are critical to survival and overall forest regeneration as seedlings are in the process of anchoring and adjusting to the stress of the intertidal environment (Lima et al., 2018; Krauss et al. 2008). Despite this, previous work on the early life-stages of mangroves have focused on mature propagules on the parent tree or already-established juveniles (Balke et al., 2011; Di Nitto et al., 2008).

In their comprehensive review on the early thresholds to mangrove establishment, Friess et al., (2012) identified crucial knowledge gaps in the literature. Specifically, they identified the lack of quantitative thresholds for mangrove seedling dislodgement at the individual scale. The influence of hydrodynamic forces (e.g. waves and currents) guide the success of mangrove colonization in these dynamic intertidal environments and threaten the success of seedling recruitment in energetic areas (Friess et al., 2012; Le Minor et al., 2019). Quantitative measurements of the vulnerability of mangrove seedlings to dislodgement from these hydrodynamic forces is needed to better understand mangrove recruitment dynamics and help ensure the successful regeneration of mangrove forests. It is assumed that high wave and current energy are limiting factors to mangrove recruitment, but specific limitations on forces these

organisms can withstand have only been identified in laboratory flume studies (Friess et al., 2012; Kamali and Hashim, 2011; Balke et al., 2011). More work is also needed to explore the effects of the local environment on guiding seedling susceptibility to dislodgement, as well as the relationship between sediment transport (e.g. deposition and erosion) and its effects on these thresholds to recruitment. As these thresholds likely differ between mangroves establishing under different abiotic and biotic conditions, quantifying the thresholds guiding recruitment in the natural environment will improve our understanding of mangrove seedlings' susceptibility to dislodgment from hydrodynamic forces.

As thresholds to recruitment become better known, one can apply these concepts to improve coastal restoration projects across the globe attempting to protect and restore mangrove habitat. The goals of these restoration efforts are to preserve mangrove habitat and utilize their intrinsic properties to mitigate issues such as shoreline erosion and sea level rise. Once lost, restoring mangrove habitat is often very difficult (Lewis, 2000). The dynamic nature of the intertidal environment causes features such as site hydrology and morphology, species, and time of planting to be crucial to restoration success. A general lack of understanding of key hydrologic processes governing the health and survivorship of mangrove forests (e.g. inundation time and wave energy) cause many restoration efforts to fail (Feller et al., 2017; Kamali and Hashim, 2011; Lewis, 2005). Incorporating research focused on mangrove establishment and early life stages into restoration practices has the potential to improve success as our understanding of mangrove establishment and forest regeneration improves.

A restoration method that has gained widespread popularity as a cost-effective, long-term solution to protect vulnerable coastlines is "living shoreline stabilization" (e.g., Gittman et al.,

2016; Gedan et al., 2011). A “living shoreline” is the stabilization of an eroded shoreline by the introduction of native vegetation and other less intrusive structures and materials, instead of seawalls or other hard armoring (Gittman et al., 2016). These methods allow the shoreline to function as it naturally would, while reducing erosion and providing habitat for native species. When creating living shorelines within the tropics and subtropics, mangroves and other halophytic plants are frequently used (Gedan et al., 2011). This is an alternative approach to many restoration projects that focus entirely on planting without considering the local hydrologic conditions, ecology of targeted mangrove species, or factors preventing natural mangrove recruitment in the area (Feller et al., 2017; Lewis, 2005). In his review of ecological engineering practices for successful mangrove restoration, Lewis (2005) notes this focus on planting is a major flaw in many restoration projects globally, and causes many programs to fail to reach specific restoration goals or fail entirely. Combining the benefits of planted mangroves with the additional benefits of other man-made structures, living shorelines help to remove specific hydrologic issues at restoration sites and act as an effective alternative to restorations exclusively using direct plantings.

When designing shoreline restoration projects, it is important to be aware of the mechanisms behind successful establishment and design monitoring schemes that are able to provide enough information to identify limiting factors (Lewis, 2000; Kamali and Hashim, 2011). Such awareness allows us to modify restoration practices to local conditions and ensure restoration sites can facilitate the natural regeneration of vegetation. Here, I identify limitations to the success of living shorelines by quantifying not only the physical limitations but biological limitations as well, in the form of propagule availability, along restored and control sites.

Through the implementation of monitoring designed specifically to measure mangrove propagule retention and recruitment, these findings address potential constraints to living shoreline stabilizations and work to improve methods to overcome them.

The goals of this project are two-fold. First, I inform on the effectiveness of a common restoration technique on increasing propagule retention and recruitment of mangroves in De Soto National Memorial (Bradenton, FL). Second, I quantify physical thresholds to mangrove recruitment by characterizing the resisting force of mangroves across various ages and biotic and abiotic conditions within two national parks at similar latitudes, De Soto National Memorial and Canaveral National Seashore (New Smyrna Beach, FL).

CHAPTER 2: MANGROVE RECRUITMENT ALONG LIVING SHORELINES

Methods

Study Site

This study was conducted along the shorelines of De Soto National Memorial (DSNM) in Bradenton, FL (Figure 1). Established in 1948, DSNM is a part of the United States National Park System. It was created to "commemorate the 1539 expedition of the Spanish Conquistador Hernando de Soto and his impact on the American Indian societies of the Southwest" (National Park Service, 2019). The Park is approximately 10.5 hectares and is located in Manatee County, Florida at the mouth of the Manatee River. DSNM contains over 914 meters of shoreline and roughly 80% of the Park area is mangrove swamp (National Park Service, 2019).

Living Shoreline Stabilization

For the purpose of this study, "living shoreline stabilization" was defined as the transplantation of plantings and ~22.5 kg mesh bags (DelStar Technologies Inc.) of disarticulated oyster shell (1 m x 24 cm x 14 cm) along vulnerable shorelines with the intention of reducing wave energy and stopping shoreline erosion. In August of 2017, 150 meters of shoreline were stabilized within DSNM (Appendix C: Figure 15). The stabilization consisted of 230 mangroves (83 *Avicennia germinans,* 147 *Rhizophora mangle*) planted in the high intertidal and 1800 oyster shell bags placed in the low intertidal (Figure 2). Planted mangroves ranged from 0.5 m to 1 m in height (*R. mangle* mean height: 65.2 ± 1.7 cm, *A. germinans* mean height: 75.3 ± 0.7 cm) and were planted a minimum of 0.6 m apart. Plants and shell bags were placed in units of 6 m with

1.5 m gaps to facilitate animal movements, especially manatees, through the structure. Unlike typical stabilizations along the east coast of Florida, *Spartina alterniflora* was not used in plantings due to its absence at this site.

Propagule Monitoring

Propagule surveying began in June 2017 and was conducted monthly until November 2018. Surveys included monitoring of propagule and seedling retention/recruitment and standing vegetation. The mangrove species of interest were the three native species to Florida: *Rhizophora mangle*, *Avicennia germinans*, and *Laguncularia racemosa*. Twelve sites were randomly selected to represent the variety of shorelines found within the park. Four sites each for natural shorelines, restored "living shorelines", and revetments were selected randomly along the shoreline of the Park. The revetments within De Soto were previously installed by park staff and are a hard-armor approach to shoreline stabilization made up of a sloped structure of large rocks and cement. Comparisons between these three categories allowed us to determine the differences in propagule availability between the Park's natural sites and sites with differing forms of shoreline stabilization methods. Due to signs of substantial erosion and related effects across much of the Park's shores, natural sites are not considered undisturbed "control" sites and were instead used as reference sites for areas without any human intervention via stabilization methods. At each site, a 10-meter transect was established parallel to the shore along the upland transition zone. Along the 10 m transect, additional transects at 0, 5, 10 m were placed perpendicular to the water's edge and used to survey mangrove propagules/seedlings and vegetation/groundcover. Along these three transects, 0.25 m^2 quadrats were placed every meter from the top of the upland

transition zone to the mean low water line. The length of transects differed depending on the physical characteristics of specific shoreline sites. To account for inherent pseudoreplication within the shoreline transect design, 10 additional quadrats were randomly selected within this area and surveyed with the same method to act as independent samples of propagule abundance. Transect surveys served to measure propagule/seedling abundance over the tidal gradient while the random quadrat sampling was used to independently measure propagule/seedling abundance across the entire site. Randomized quadrat surveys started after the shoreline transects and only include the 2018 propagule season. All mangrove propagules and seedlings within each quadrat were counted. Groundcover surveys were conducted with the point intercept method (Caratti, 2006) within each quadrat. A total of 25 points were established in each quadrat. Groundcover and vegetation, identified to species, were recorded at each of these points to determine percent coverage within the quadrat. Averaged groundcover values characterizing all shoreline types can be found in Table 1.

Statistical Methods

Propagule counts were analyzed through generalized linear model (GLM) selection. The response variable for all models was the total number of live propagules within the 0.25 m^2 quadrat while predictor variables tested included shoreline type (restored, natural, or revetment), percent of surrounding vegetation, month surveyed, and location within the park (West/East shore). Data was analyzed though likelihood-based model selection. Alternative models were compared and ranked using the corrected Akaike Information Criteria weights (AICc) from the R package “bbmle” (Bolker et al., 2017). Due the low number of propagules of different species at

many sites during monitoring, all species were grouped for analysis. Additionally, months where no propagules were observed at any sites and that were outside of typical mangrove propagule release season (July-November), were excluded from the analysis to remove excess zeros from the dataset. To correct for inherent pseudoreplication within the transect survey design, propagule counts were averaged across transects and sites. This averaged value was then rounded to the nearest integer for analysis. Through this process some information was lost, however, it was a necessary step in order to analyze the data appropriately. The 10 additional random quadrats at each site were treated as independent samples during analysis and modeled separately. Alternative models for both transect survey data and randomized quadrat data were modeled with both Poisson and Negative Binomial errors to account for the nature of the count data and the high abundance of zeros within the dataset. Residuals of models constructed with Poisson and Negative Binomial error distributions were verified in part with the DHARMa package in R (Appendix C: Figure 21) (Hartig, 2019). The DHARMa package uses simulated, standardized model residuals to provide interpretable plots in order to check for patterns in residuals or evidence of over/underdispersion in generalized linear models. All statistical analyses were performed with R 3.5.1 software (R Development Core Team, 2018). All graphs were constructed using the "ggplot2" package in R (Wickham, 2009). Tables of model results were constructed with R package "stargazer" (Hlavak, 2018) and Microsoft Excel (2013).

Results

Mangrove propagule recruitment peaked in August and September of 2018. With maximum wind speeds of 92 mph, Hurricane Irma likely had negative effects on propagule

counts conducted in the 2017 propagule season, as shown by the markedly reduced propagule counts in September of 2017 when compared to the subsequent year (Figure 3). Due to park closures associated with hurricane damage, we were unable to perform propagule surveys in August 2017. August and September showed the highest propagule abundance of all months surveyed in 2018. The average propagule counts for shoreline transects surveys peaked in September 2018, with restored shorelines showing an average of 23.9 (± 5.0) propagules per 0.25 m^2, followed by natural shorelines (4.7 ± 1.1), and revetments (0.2 ± 0.1). Model selection results for the transect surveys can be seen in Table 2. The most plausible model was a generalized linear model with a negative binomial error distribution that included the abundance of propagules as a function of the additive effects of shoreline type, month surveyed, surrounding vegetation cover, and location within the park (model 2; Table 3). This model shows propagule counts for natural sites were significantly lower than in restored areas (GLM: $p = 0.01$). Additionally, natural and restored shorelines showed larger propagule counts than what was found at revetment sites (GLM: $p < 0.001$). Most sites had very little recruitment while few sites showed a substantial number of propagules. Of the 12 sites surveyed, just two sites, Restored 1 and Natural 1, were responsible for the significantly larger propagule counts within the months of August and September of 2018; both sites were found along the West shore (Appendix C: Figure 19). These sites had a greater influence on the overall average number of propagules seen along each shoreline type. More propagules were found at the Natural 1 site than all other sites except for Restored 1 (Appendix C: Figure 19).

The results of the randomized quadrat survey are congruent with the shoreline transect survey. Survey results show that mangrove propagule abundance peaked, as expected, during the

months of August and September (Figure 4). Overall, the average propagule count for restored shorelines surveyed with randomized quadrats peaked in August 2018 with 8.3 (± 3.2) mangroves per 0.25 m^2, followed by natural shorelines (3.3 ± 1.0) and revetments (0.1 ± 0.1). Model selection results for the randomized quadrat surveys can be seen in Table 4. The most plausible model (model 7) was a generalized linear model with negative binomial error distribution that modeled the abundance of propagules as a function of the additive effects of shoreline type, month surveyed, and location within the park. As seen in the shoreline transect survey, there was considerable variation between shoreline types during the propagule season (Table 5). Restored shorelines showed greater propagule recruitment than both natural and revetment sites (GLM: $p < 0.001$). Natural shorelines showed greater propagule counts than revetment sites (GLM: $p < 0.001$). Again, we see most sites had very low propagule counts per 0.25 m^2, while sites Restore 1 and Natural 1 had much larger mean propagule counts.

Percent cover of surrounding vegetation for the shoreline transect surveys was found to have a slight positive effect on propagule abundance ($p < 0.05$; Table 3). This effect was not seen in randomized quadrat surveys and was not included in the final model configuration. The low vegetation groundcover levels present across all shoreline types (Table 1) likely limit the impact of vegetation on increasing propagule retention. Average vegetation groundcover was below 9% along natural areas and ~3% in restored areas despite most propagules being found along those shorelines. The vegetation cover along natural shorelines and restored shorelines consisted primarily of *A. germinans* pneumatophores. Vegetation at revetment sites was seagrass (*Halodule wrightii*) in the shallow subtidal. The effect of vegetation is overshadowed by the significantly greater propagule abundance seen at survey sites located along the West shore for

both shoreline transect and randomized quadrat surveys (GLM: $p < 0.001$; $p = 0.002$). Aside from shoreline type and month surveyed, a site's location on either the West or East shores of the park was shown to have the greatest influence on propagule abundance.

As made clear through 16 months of shoreline surveys, there was little mangrove recruitment along the sampled shorelines of De Soto National Memorial (Figures 3, 4). Over the course of the randomized quadrat surveys, a total of 18 mangrove seedlings were found along natural shorelines. Six seedlings were found along restored shorelines, while five were present at revetment sites. Seedlings found at the natural and restored sites were generally associated with other vegetation or shell bag structures, while seedlings along revetments were found growing in-between the large boulders making up the hardened shoreline. Due to insufficient number of seedlings found, no formal analyses were conducted on differing seedling abundances across sites. It is clear through the raw data that there was limited seedling establishment across all sites surveyed (Figures 3, 4).

Discussion

One of the biggest limiting factors in successful mangrove restoration projects is sustained natural recruitment post-restoration (Lewis, 2005). To reduce initial planting and maintenance costs, restoration designers must be aware of the history and potential of propagule availability at restoration sites and surrounding areas. Understanding the local propagule stock allows researchers and resource managers to modify restoration designs or increase initial planting(s), as well as make predictions on the regenerative potential of restored areas (Bosire et

al., 2008). Restoration efforts may even be able to skip planting entirely if a local propagule stock is sufficient and the physical limitations stopping natural regeneration are removed.

There was substantial variation in the propagule availability across De Soto National Memorial's shorelines. Through 16 months of shoreline surveys, the main drivers of propagule abundance are shown to be seasonal variation and site-specific factors. In this study, segments of shoreline within a small area (914 m of Park shoreline) were shown to receive different propagule abundances, influencing recruitment and future growth. De Soto's proximity to popular boating channels, at the connection between the Manatee River and Tampa Bay, may add additional physical stressors to recruitment than wouldn't naturally be present. As wave intensity and frequency increases with boating activity (Sheremet et al., 2013), increases in the hydrodynamic energy, from wave and current forces, will apply more stressors on propagule establishment through increased inundation time and drag forces (Friess et al., 2012). This increasingly dynamic system could be leading to more variation in propagule distribution as propagules are dislodged before anchoring or potentially stranded beyond suitable shoreline habitat into upland areas. Donnelly and Walters (2008) showed experimentally that invasive *S. terebinthifolius* (Brazilian pepper) seeds were deposited significantly higher along shorelines by boat wakes compared to naturally generated wind wakes in Mosquito Lagoon, Canaveral National Seashore, allowing them to successfully establish well-above the mean high tide. While *S. terebinthifolius* dispersal benefits from increased wave action, mangrove establishment may be hindered by movement outside of suitable intertidal habitat.

As seen in this study, two survey sites (Natural 1, Restore 1) showed considerably larger propagule counts than neighboring shorelines with similar physical features. This difference in

propagule abundance was not driven entirely by factors we directly tested (shoreline type, vegetation cover) but instead appears to be driven mostly by their close proximity to mature mangrove trees (*Avicennia germinans*, *Laguncularia racemosa*). Mature mangrove trees were visually observed to be more prevalent along the Western shore of the Park, coinciding with the site location's strong effect on increasing propagule abundance (Table 3, 5). Severe erosion along the shorelines of De Soto have left mangrove coverage limited in many areas. While mature mangroves are present along other survey sites, it appears there are differences in propagule contribution and other factors (e.g. elevation, local hydrology) (Sousa et al., 2007; Delgado et al., 2001; Van der Stocken et al., 2019), beyond what we surveyed for, that are limiting the distribution of propagules between sites. While looking at survey results would indicate restored areas showing greater mangrove recruitment, in actuality, these differences are driven by site-specific factors, such as the presence of mature mangroves, as opposed to the effects of differing stabilization methods.

While the presence of mature trees leads to more propagules within the area, vegetated groundcover has a limited effect on site-specific propagule retention and recruitment within De Soto. While vegetation was shown to slightly increase propagule abundance along the shoreline transects, no effect was seen in the randomized quadrat surveys. This is likely due to the overall lack of vegetation along much of De Soto's shorelines (Table 1) due to the effects of prevalent erosion and wave damage. This lack of vegetation, and generally low propagule counts overall, could be limiting our ability to characterize this relationship. The vegetation that is present is highly localized, contrary to less disturbed natural shorelines in adjacent areas where mature mangroves form homogenous stands with dense pneumatophore coverage. These "hotspots" of

vegetation, characterized by dense root structures, appear to be grouped around mature mangrove trees that have not succumbed to the effects of erosion. Additionally, vegetation cover in restored sites is still very low, as these restorations are <2yrs old. As these sites begin to mimic natural mangrove systems in their structural complexity, these results may change. Dense stands of vegetation in mangrove forests have been shown to have positive effects on propagule recruitment as these complex structures act to "trap" stranded propagules in the area (Donnelly et al., 2017; Robert et al., 2015; Sousa et al., 2007; Lewis, 2005). Additionally, natural recruitment often increases with the age of restored areas (Bosire et al., 2008). While the living shoreline installed in De Soto has shown signs of success in terms of mangrove survival and oyster recruitment on bagged shells (Appendix C: Figure 16-18), the true effect of restoration on mangrove recruitment will likely not be seen until vegetation at these sites grow in size and complexity, directly trapping propagules and further reducing shoreline energy.

The presence of naturally-recruited seedlings is very limited along De Soto's shoreline. This holds true for all survey sites, even Restore 1 and Natural 1, where the highest propagule counts were observed. These densities mimic seedling densities observed by Carlos et al. (2015) of <0.35 seedlings per m^2 in disturbed mangrove habitat in the Philippines, following damage from Typhoon Haiyan. Excessive wave force and erosion along De Soto's shorelines may be driving these patterns of low recruitment and further demonstrate the importance of understanding the reasons behind lack of recruitment when designing restoration projects (Kamali and Hashim, 2011; Lewis, 2005). This distinction between the large amount of propagules available in parts of the system and the lack of natural recruitment suggests that there are other factors that are limiting the successful establishment of mangroves. In areas where

biological constraints seem unlikely, we can begin to explore the potential presence of physical limitations to recruitment.

CHAPTER 3: HYDRODYNAMIC LIMITATIONS TO MANGROVE RECRUITMENT

Methods

Greenhouse Design and Care

To understand how the rooting strength of *A. germinans* and *R. mangle* changes with age and sediment type, testing was first focused on a controlled setting by growing mangrove seedlings in a greenhouse environment before conducting tests in the field. Propagules of both species were collected from trees in Canaveral National Seashore in September of 2017 and planted in 1-gallon plastic planting pots in a hoophouse at the University of Central Florida. Locations of all pots were randomized within the growing space and filled flush with sediment before planting. 1-gallon pots were contained in larger 15-L plastic tubs to maintain constant submersion in water. Each tub was watered to a 23 cm depth weekly. A total of 18 tubs were used, each containing 10 1-gallon pots. The greenhouse experiment consisted of two sediment treatments of "fine" and "coarse" sediment. The fine sediment treatment consisted of 50% commercial "play sand" and 50% crushed oyster shell (D84: 3.18 ± 0.97 mm; D50: 0.37 mm ± 0.02; mean shell size: 1.5 ± 0.2 cm), while coarse sediment treatment consisted of 50% fine commercial "play sand" and 50% large, intact oyster shells (D84: 13.16 mm ± 4.98; D50: 0.44 mm ± 0.05; mean shell size: 5.9 ± 0.3 cm). Each mangrove species was grown for 1, 3, or 4 months, with 15 mangroves per sediment treatment and time interval used in trials.

Seedling and Sediment Characterization

Seedling morphometric variables collected for both greenhouse and field samples are provided in Tables 6 and 7. Seedling size was further characterized through "frontal area", calculated using the method described in Lightbody and Nepf (2006) using a digital camera with a white background with vertical and horizontal scale bars. Images were processed through ImageJ image processing and analysis software (ver. 1.46r). After removal from the sediment, weights of seedling wet and dry above and below-ground were obtained to estimate their biomass. Detached root mass was retrieved from sediment after each pull-test.

The sediment grain size distribution was quantified for both greenhouse and field experiments using dry sieving with mechanical shaker. Wet sieve analyses on sediment subsamples were also conducted for field sediments and combined with the results of dry sieve analyses. Standard sieve sizes ranging from 76.200 mm to 0.074 mm were used (Liu and Evett, 2008). A subset of fine and coarse sediments used in the greenhouse pull-tests were used to quantify grain size (mean dry mass: 3207.28 g ± 611.92 g). For field tests, five sediment samples were taken from each mangrove sampling location to a depth of 10cm using an acrylic core (diameter of 10cm). Samples were then aggregated (mean dry mass: 637.36 g ± 138.52 g) and analyzed for grain size as well as additional measurements of sediment organic matter through loss on ignition tests. Loss on ignition tests were conducted by passing the sample through a 2.00 mm sieve, heating a subsample (20g) to 550°C in a muffle furnace for 16 hours, and calculating percent organic matter lost. Summary parameters were computed using the grain size distribution and include the D84 and D50. The D84 is defined as the size of the particle where 84% of the sample is finer by weight. D50 is defined similarly.

Lateral Pull-Test Design

Lateral pull-tests were used to simulate hydrodynamic forces and measure the resistance of mangrove seedlings to uprooting from hydraulic forces similar to those experienced in their natural environment. These tests were used to measure the resistance force, the threshold to dislodgment, by taking the horizontal component of the force applied in a manner that is portable and reproducible in the field (Bywater-Reyes et al., 2015). Pull-test methods were adapted from Bywater-Reyes et al., (2015) with pioneer riparian vegetation (*Populus* spp., *Tamarix* spp.).

For all lateral pull-tests, seedlings were uprooted by attaching each mangrove to an anchored hand-winch using a 4.8 mm nylon rope loop around the base of the seedling. This was then attached to a 3.2 mm steel wire rope and pulled laterally until removal from sediment (Figure 5). The force exerted on each seedling was continuously measured (every 0.5 seconds) using an Omega environmentally protected load cell (max= 111 N; error = 0.25%) and logged using a Campbell Scientific CR850 data logger. Pull-test methods were performed on mangroves grown in a greenhouse environment as well as mangroves found *in situ* (Figure 6).

The horizontal resistance force (F_D), or horizontal force to removal, of each mangrove seedling was calculated with equation 1. This allows us to compare the forces applied (F_A) by the lateral pull-test to horizontal drag forces experienced naturally.

$$F_D = F_A * \cos(\Theta) \quad (1)$$

Greenhouse pull-tests were complimented with *in situ* lateral pull-tests at two locations on the east and west coasts of Florida, Canaveral National Seashore and De Soto National Memorial, respectively (Figures 7, 8). Pull tests were conducted from May through August 2018. At each Park, 50 *R. mangle* and 50 *A. germinans* seedlings were haphazardly selected from the

sample areas. To acquire the necessary number of seedlings while testing a variety of sediment types, a minimum of two separate sample locations were selected within each Park. Due to the absence of adequate locations containing both *R. mangle* and *A. germinans* at De Soto National Memorial, three sampling locations were needed. Only *R. mangle* seedlings were tested at the De Soto 1 site while only *A. germinans* seedlings were tested at De Soto 2 site. The third site was handled normally with both species being tested. Twenty-five seedlings were sampled from each location. Mangroves were sampled at high tide with seedlings found within standing water, ensuring the sediment surrounding each seedling was saturated during each pull-test. Groundcover surrounding each seedling was quantified prior to performing the treatment through the point intercept method (Caratti, 2006) within a 0.25 m^2 quadrat centered on the seedling. All species of vegetation within the quadrat were counted and identified to species level. Canopy absence or presence was quantified using a GRS densitometer directly above each seedling and at four separate right angles from the seedling, allowing for the binary response of canopy presence/absence at a total of 5 locations immediately around the seedling.

Statistical Methods

Potential environmental and morphometric effects on the force required to uproot mangrove seedlings were modeled using generalized linear models. The response variable for all models was the horizontal force to removal (Eq. 1). For the greenhouse experiments, predictor variables tested include species, age, above/below-ground biomass, seedling height, seedling frontal area, and sediment treatment. Data was analyzed though likelihood-based model

selection. Alternative models were constructed and compared via corrected Akaike Information Criteria (AICc) and Akaike weights from the R package "bbmle" (Bolker et al., 2017).

For pull-tests conducted in the field, the predictor variables tested include species, above/below-ground biomass, seedling height, leaf number, base-diameter, seedling frontal area, sediment grain size, and percent sediment organic matter. Alternative models were compared and ranked using the corrected AICc weights and further evaluated based on residual plots.

While creating the candidate models for both greenhouse and in-field pull tests, alternative measures of plant size were used. Due to collinearity, however, only one of these variables was used in any candidate model. Including multiple measures of plant dimensions allowed us to determine which morphometric variables were most useful in predicting a seedling's resistance force while creating a model with relevant estimates useful for management decisions. All statistical analyses were performed with R 3.5.1 software (R Development Core Team, 2018) . All graphs were constructed using the "ggplot2" package in R (Wickham, 2009). Tables of model results were constructed with R package "stargazer" (Hlavak, 2018) and Microsoft Excel (2013).

Estimating Velocities

To contextualize these findings, we can use the horizontal force to removal values provided in this study to calculate the velocities where our sampled mangrove seedlings from the field would become susceptible to uprooting due to hydrodynamic drag forces in the context of a short duration flow event and in the presence of no erosion around the seedling base. The hydrodynamic forces experienced by seedlings under wave and current flows can be

parameterized as a drag force (F_D; Equation 2) where ρ is the density of seawater (1030 kg/m^3), C_D is the drag coefficient, A_C is the frontal area of the seedlings, and U_C is the approach velocity. By equating the drag force (F_D) to the resisting force (F_R) of seedlings, we can calculate the critical velocities where mangrove seedlings would become vulnerable to uprooting in their natural environment (Bywater-Reyes et al., 2015).

$$F_D = 1/2pC_DA_CU_C^2 \quad (2)$$

We do this by solving for the velocity term and using measured values from our field pull-tests for resisting force and frontal area (Equation 3).

$$U_C = \sqrt{\frac{2 * F_R}{\rho C_D A_C}} \quad (3)$$

The literature was reviewed to find appropriate drag coefficients that were realistic for mangrove forests. A recent study by Le Minor et al. (2019) used numerical models to simulate the flow pattern and sediment dynamics around individual mangrove seedlings. They utilized a drag coefficient equaling 1 and a simulated seedling with an average diameter of 1 cm and height of 12.4 cm tested under velocities of 5, 10, 15, and 50 cm/s, within the range of velocities measured in areas surrounding our Canaveral field sites. Their numerical model was validated against velocity profiles from flume data on flow around a vertical cylinder. They analyzed drag forces for all velocities and validated them against theoretical values provided by Mullarney and Henderson (2017), finding their estimated forces were in good accordance with the theoretical ones (Le Minor et al., 2019). This drag coefficient of 1 is comparable to other coefficients estimated through flume tests with modeled mangroves (low C_D= 0.98, high C_D= 1.14; Struve et al., 2003) and fell within the range of in-field C_D values measured (0.4-10) across a variety of

mangrove habitats within Australia, Japan, and Vietnam (Mazda et al., 2005). With this support, we chose to calculate critical velocity values utilizing a drag coefficient of 1. The frontal area term (A_C) in equation 3 was calculated by taking the frontal area of sampled seedlings and applying a reduction coefficient to account for pronation or the streamlining of leaves in response to hydrodynamic forces. A normal distribution of possible reduction values was created with a mean of 0.7 and a standard deviation of 0.1 (ranging from 0.4 to 0.95) and were randomly assigned to each mangrove seedling. This represents that seedlings were more likely to reduce their frontal area by 70% under hydrodynamic forcing.

Results

Greenhouse Lateral Pull-tests

Due to mangrove mortality during greenhouse cultivation, 177 out of 180 mangroves were tested in the greenhouse pull-tests. Of those tested, 11 individuals displayed higher forces to removal than our instrumentation could measure (exceeding 25 lbf) and were not considered in the analysis, but were examined qualitatively; 166 mangroves were thus used in the analysis. Below-ground biomass was shown to be the best metric of plant size at predicting the horizontal force to removal and was used for all later alternative greenhouse models. The data are most effectively modeled using linear regression after natural log transformation of the response variable: horizontal force to removal. The chosen linear model outperformed alternative models with differing model configurations fit with both Gamma and Gaussian distributions (Table 8). The data were modeled with a linear regression that modeled the horizontal force to removal as a function of the interaction between below-ground biomass and species and an interaction

between age and sediment treatment (Model 9; Table 9). Based on residual plots, this model was shown to have minor deviations from normality (Appendix C: Figure 32), but was chosen as the most plausible out of the set of alternative models.

R. mangle seedlings had a significantly greater force to removal then *A. germinans* seedlings, by 0.94 N (95% CI: 0.65, 1.22) on average. A 0.20 N (95% CI: 0.13, 0.27) increase in horizontal force to removal was seen with increases in below-ground biomass (GLM: $p < 0.001$). Both species of mangroves showed positive increases in horizontal force to removal with increased below-ground biomass (Table 9, Figure 9). Despite this, the force to removal of *A. germinans* and *R. mangle* seedlings increased at different rates. The increase in force to removal of *R. mangle* seedlings was significantly reduced by -0.13 N (95% CI: -0.20, -0.06) when compared to *A. germinans* seedlings.

As expected, the age of mangroves was shown to have a significant effect on force to removal. Compared to 1-month-old seedlings, the average horizontal force to removal for the 3 month treatment was greater by 0.76 N (95% CI: 0.56, 0.95) and 4 month treatment by 1.02 N (95% CI: 0.82, 1.21). The fine sediment treatment was shown to have a significant positive effect (GLM: $p = 0.03$) with the force to removal of seedlings grown in the fine sediment treatment increased by 0.28 N (95% CI: 0.10, 0.46) on average. Despite this initial positive effect, a slight negative effect (GLM: $p = 0.008$) is seen in the 4 month treatment showing reduced horizontal force to removal. However, the large overlap in confidence intervals (Figure 9) indicates this effect is small. As seen in Figure 10, the difference in force to removal between sediment treatments is greatest in the first month.

Field Lateral Pull-tests

A total of 95 *R. mangle* and 87 *A. germinans* were sampled in the field. Through model selection, above-ground biomass was shown to be the best metric of plant size in predicting the horizontal force to removal and was used for all later alternative field models. Sediment characterization indicates that while median grain sizes were similar across sites, contents of silt, clay, and particulate organic matter varied substantially among sites (Table 10). Field sediments are much finer than sediments from greenhouse pull-tests as field samples were taken from the interior of mangrove islands/forests, unlike sediments found along exposed shorelines.

The data are most effectively modeled using a linear regression after natural log-transformation of the horizontal force to removal. Through model selection, the top models were identified to be models 4 and 6 (Table 11). As they have ΔAICc values less than 2, there is no evidence of a strong distinction between them. By evaluating model results, the "Park" factor was not found to have a significant effect and model 4 was chosen (Model 4, Table 12).

Horizontal force to removal increased by 0.21 N (95% CI: 0.12, 0.32) with increases in above-ground biomass (GLM: $p < 0.01$) (Figure 11). A significant difference (GLM: $p < 0.003$) between species was also found, with the force to removal of *R. mangle* seedlings being greater by 0.52 N (95% CI: 0.17, 0.83) on average. There are inherent differences between the biomass of these species during this early life stage that drive differences in force to removal. The mean (± S.E.) above-ground biomass of *A. germinans* seedlings was 1.83 ± 0.11g, while *R. mangle* seedlings were much larger (21.16 ± 0.86g). Looking at the interaction effect between above-ground biomass and species in model 4 (Table 12), we can see that the force to remove *A. germinans* seedlings increased in response to increases in biomass at a faster rate (0.21 N, 95%

CI: 0.12, 0.32) than what is seen in *R. mangle* seedlings (p = 0.001; Table 12; Figure 11). The rate at which the force to removal increased for *R. mangle* seedlings was reduced by -0.18 N (-0.28, -0.08) when compared to *A. germinans* seedlings. Using the model coefficients, we can create a regression equation and estimate the horizontal force to removal for both *A. germinans* and *R. mangle* seedlings. The relationship between horizontal force to removal and biomass is described by equation 4 for *A. germinans* seedlings and equation 5 for *R. mangle*.

$$\text{Horizontal Force to Removal} = e^{(2.43 + 0.22*\text{Above-ground Biomass(g)})} \quad (4)$$

$$\text{Horizontal Force to Removal} = e^{(2.9 + 0.04*\text{Above-ground Biomass(g)})} \quad (5)$$

The influence of mangrove species and above-ground biomass on force to removal is consistent across De Soto and Canaveral as no significant effect was seen between mangroves sampled from different Parks. Vegetation and canopy cover values measured directly around each sampled mangrove were not found to have a significant effect on the horizontal force to removal for either species. However, slight positive trends (not significant) were seen in the force to removal of *A. germinans* seedlings growing in more vegetated areas. This trend was consistently positive for *A. germinans* while the highest force to removal values for *R. mangle* were grouped around areas with intermediate vegetation cover (Appendix C: Figure 26). Canopy cover was not seen to have a significant effect on resistance. *R. mangle* seedlings sampled in heavily canopied areas show greater variability in their force to removal when compared to seedlings growing in more open areas (Figure 12). This relationship was not seen in *A. germinans* seedlings.

Velocity Estimations

Using equation 3 and the values provided by the lateral pull-tests conducted in the field, we calculate the velocities where our sampled mangroves would become susceptible to dislodgement due to hydrodynamic forces. It is important to note that these are estimated within the context of a short duration event where no erosion has taken place around the base of the mangrove seedling. Within this context, *R. mangle* seedlings from our field tests are predicted to be susceptible to dislodgement under velocities of 5.40 ± 1.59 (S.D.) m/s. *A. germinans* seedlings would become susceptible to dislodgement at velocities of 7.33 ± 2.07 (S.D.) m/s. As these two mangrove species display large differences in size, and therefore frontal area, drag forces experienced by seedlings will differ greatly. If we only look at frontal area sizes where the two species overlap, the critical velocities are calculated to be 6.66 ± 1.23 (S.D.) m/s for *R. mangle* and 6.25 ± 1.58 (S.D.) m/s for *A. germinans* seedlings.

Discussion

Lateral Pull-tests

Submerged and emergent vegetation occupying coastal environments are threatened by dislodgment from hydrodynamic forces if the drag forces experienced surpass the resisting force of their roots. Despite the far-reaching implications on mangrove dispersal, regeneration, and long-term success of mangrove restoration, little is known on the physical thresholds that guide successful mangrove recruitment. By quantifying how seedlings' susceptibility to dislodgement varies through time and across differences in size, we inform on the physical conditions under

which successful recruitment can be expected, adding to the literature and providing a more holistic view of the mechanisms behind seedling establishment.

The general relationship between biomass levels and force to removal was consistent across both field and greenhouse pull-tests. The greater average force to removal in greenhouse samples are due to differences in growing conditions and sediment saturation. Growing in isolation and facing no competition for sunlight or nutrients likely led to the increased below-ground biomass levels in the 3- and 4-month treatment, and subsequently force to removal. Additionally, due to the nature of testing seedlings grown in a greenhouse environment, the sediment in the greenhouse pull-tests was not fully saturated before each pull-test and has the potential to affect the force to removal. While full saturation was not achieved, saturation levels were similar to previous work testing the force to removal of riparian vegetation (Bywater-Reyes et al., 2015).

Below-ground biomass was more closely related to force to removal for greenhouse trials while above-ground biomass was a better predictor for field tests. Nutrient levels were likely lower in greenhouse sediment (crushed, washed silica "play sand") when compared to relatively nutrient-rich sediment typical of mangrove forests along river outlets and lagoons (Feller et al., 2007). Low nutrient/high light conditions likely caused increased below-ground biomass stock seen in greenhouse seedlings (McKee, 1995; Simpson et al., 2017), leading to greater below-ground biomass levels overall and increased force to removal. With seedlings in the field, older than 4 months and growing in more shaded, crowded environments, growth is likely focused towards above-ground fractions as competition for light is more common (Poorter and Nagel, 2000). Additionally, lower below-ground biomass levels may also be caused by the more

nutrient-rich field environments. Recent work has shown that nutrient enrichment causes increased above-ground biomass production in comparison to below-ground stock in the mangrove, *Bruguiera sexangula* (Gillis et al. in rev.). For seedlings sampled from the field, the greater above-ground biomass seen in *R. mangle* seedlings and lower below-ground biomass in both species likely makes above-ground biomass a better indicator of plant age, and subsequently anchoring ability, for field pull-tests.

A. germinans seedlings show a greater increase in force to removal with increases in biomass, when compared to *R. mangle* samples for both greenhouse and field tests. Due to differences in the size at early life stages, the resistance force of *R. mangle* seedlings is initially greater. However due to the different rates of increase between species, *A. germinans* seedlings show higher force to removal as they produce biomass levels comparable to that of *R. mangle* seedlings (Appendix C: Figures 24;25). This may be initially true for early life stages, before differences in mature root morphology (ex. the cable roots of *A. germinans* and prop roots of *R. mangle*) complicate this relationship. Conducting additional pull-tests on seedlings of varied ages and sizes will allow us to see if this relationship stays consistent throughout the seedling phase.

Previous studies indicate root morphometric variables — length, density, and frontal area — have a positive influence on force to removal of *Tamarix* and *Populous spp.* in other riverine systems (Bywater-Reyes et al., 2015; Pasquale et al., 2013). In our study, root breakage during pull-tests lead to difficulties measuring the relationship between these variables and force to removal. Going forward, a subset of suitable mangrove seedlings could be sampled to determine allometric relationships between these variables and above-ground measures of size and test their effects on force to removal.

The coarse sediment treatment used in the greenhouse pull-tests has a larger coarse fractions than sediment found at any of our field sites, indicated by large D84 values (Figures 29, 30). The coarse fraction of the fine sediment treatment is larger than all field sites except for De Soto 2. Larger coarse fractions were used to test our hypothesis that larger grain sizes would lower the force to removal of mangrove seedlings in an environment where we had full control. Additionally, these larger sediment grain sizes are common across the open shorelines of field site locations as Native American shell middens can be found along the shores of both Canaveral National Seashore and De Soto National Memorial (Donnelly et al., 2017). Our sediment trials showed fine sediments had a small positive effect on force to removal in the 1-month age treatment that lessened through time. This effect may indicate that these differences in sediment characteristics only noticeably affect the force to removal in the very early stages of development. Previous work has shown evidence for the force to removal of *R. mangle* seedlings established in rubble to be greater than seedlings growing in sand or peat, but this is likely due to the burial of the seedlings' stems in these large, rocky sediments and not solely a result of rooting strength (Boizard and Mitchell, 2011). Additionally, coarser sediments have a negative effect on biomass production (Duarte et al., 1998). Larger sediment grain sizes can reduce a seedlings ability to resist drag forces as well as potentially limit the successful establishment of mangroves initially by obstructing anchoring, as the surface layer is more mobile and difficult to penetrate (Donnelly et al., 2017). However, grain size may have limited effects on older seedlings, where roots extend deeper. Sediment treatments consisting of homogenous, coarse sediments could be used in the future to explore the extremes of this relationship and model

different shoreline environments as increased wave energy generally leads to the displacement of finer sediments (Garel et al., 2008), leading to larger coarse fractions.

The force to removal of seedlings from our in-field pull-tests showed a similar relationship (Figure 13) to sediment grain size. The coarse fraction of sediment samples (D84; Table 10) was relatively consistent across most sites. Field sites where only one mangrove species was sampled (De Soto 1 for *R. mangle* and De Soto 2 for *A. germinans*) were the only sites to have larger D84 values. While the force to removal of *A. germinans* seedlings did not seem to be affected by changes in the coarse fraction, *R. mangle* seedlings from the field site with the largest coarse fraction (De Soto 1) displayed the lowest average force to removal. These results indicate a varying response to sediment grain size that is not consistent across species. The force to removal of *R. mangle* seedlings is much more variable across changes in sediment grain size. These differences could be related to the difference in size of these two species and how their differing root-mass interacts with the surrounding substrate. However, while we are able to look at the potential effects of sediment characteristics qualitatively, confounding site factors may also be playing a role as sediment grain size was characterized at each site and not at an individual scale.

We did not find significant relationships between canopy cover and surrounding vegetation on a seedlings force to removal. However, previous studies examining the effects of vegetated habitat on reduction of current and wave velocities within mangrove stands (Shan et al., 2019; Hortsman et al., 2012) and other coastal wetlands (Bouma et al., 2005) show evidence that these factors can influence the stability of establishing seedlings. In the current study, *A. germinans* seedlings showed a slight positive trend in force to removal as the surrounding

vegetation coverage increased (not significant) while *R. mangle* seedlings appeared to have the greatest force to removal at intermediate vegetation levels. The root-root interaction between establishing mangroves and the surrounding vegetation can increase force to removal and reduce uprooting susceptibility (Boizard and Mitchell, 2011). The effects of vegetation cover in the understory of mangrove forests can be complimented with the influence of a dense overstory. *R. mangle* has been characterized as shade-intolerant (Ellison and Farnsworth, 1993) with low-light levels having the potential to limit growth (Lima et al., 2018; Boizard and Mitchell, 2011). While no significant effect was found, the increased variation seen in the force to removal of *R. mangle* seedlings (not seen in *A. germinans*) under denser canopy levels in our study could point to a possible relationship between canopy cover and force to removal. Previous work shows greater successful long-term establishment of mangrove species under an open canopy as seedlings have better access to resources, which in turn can effect growth and uprooting susceptibility (Minchinton, 2001). Additional tests with larger samples sizes are needed in our study system in order to provide more substantial evidence for these potential relationships.

Susceptibility to Natural Dislodgment

The critical velocities calculated in the current study are over-estimations, representing uprooting susceptibility under direct forcing, and do not reflect other modes of failure. Natural mangrove failure and dislodgement will likely occur in the presence of sediment erosion in these dynamic environments instead of discrete periods of forcing from waves and currents (Le Minor et al., 2019). Erosion around the base of mangrove seedlings will lower the resisting force of their roots and therefore reduce the drag forces needed to uproot (Bywater-Reyes et al., 2015).

However, these estimates give us a baseline for direct mangrove failure and begin to characterize this relationship.

We can put our critical velocity values into ecological context by comparing our values to measured field velocities. While data is lacking concerning the velocities of large boat wakes and current flows impacting De Soto's shorelines, significant wave heights were measured within the Park on July 2, 2018 and provide an indication of the wave environment (Figure 14). Previous work conducted in Canaveral National Seashore, within 3.2 linear kilometers from our Canaveral field sites, have quantified onshore wave and current velocities at vegetated sites and sites with constructed seawalls using a Vectrino Profiler (Nortek) with a sampling rate of 100Hz. Mean onshore velocity values at reference sites were 0.6 cm/s with peak velocities of 19.0 cm/s. Seawall sites show mean onshore velocities of 1.2 cm/s and peaks of 23.6 cm/s (Kibler et al., in rev.; Spiering et al., in rev.). As mangroves occupy a variety of habitats, such as open coasts, riverine systems, and quiet lagoons, flow velocities in these diverse systems are highly variable and dependent on local conditions. While velocities in surrounding areas can be much higher, velocities within healthy forests are reduced by dense mangrove vegetation (Zhang et al., 2015). Work by Wolanski et al. (1990) in Coral Creek, Australia showed velocities in the main creek reaching 200 cm/s while velocities in the interior fluctuated around 10 cm/s due to the dense mangrove vegetation. Kathiresan (2003) observed tidal flows of 18-20 cm/s in areas lacking mangroves while areas with mangroves present showed velocities of 0-9 cm/s. Although reduced in the interior, velocities are increased at the wave/current-exposed fringes (Le Minor et al., 2019) and place new, colonizing mangrove seedlings at risk from these higher forces. Additionally, the increases in the frequency and intensity of breaking waves along exposed areas

could create new threats to mangrove establishment through sediment loss and root breakage, consequently lowering seedling resistance force. The increased stressors seen along these exposed fringes could indicate why seedling establishment is low in areas like De Soto, despite an adequate propagule supply. Note, however, velocities measured in these environments are an order of magnitude lower than our calculated velocities. The higher range of our critical velocities will likely not be reached in most systems. However, these velocities do not tell the whole story. While these measurements are able to characterize baseline conditions, such as tidal flows and wakes from wind and small boats, they do not provide information on velocities seen during extreme events such as storms or wakes from large vessels. The velocities created by these extreme events will likely exceed the magnitude seen in normal tidal and current flows. Fritz et al. (2006) estimated onshore velocities of the 2004 tsunami in Indonesia, reaching magnitudes of 2-5 m/s in urban areas more than 3 km from the coast. Velocities seen in exposed coasts and islands likely reach higher magnitudes. These velocities in combination with the effects of erosion and root breakage may leave establishing seedlings susceptible to dislodgement. Anthropogenic stressors can add to these natural disturbances, placing establishing mangroves further at risk. As recreational boating increases across areas of Florida (Donnelly et al., 2017), popular coastal areas, like De Soto National Memorial and Canaveral National Seashore, are threatened by increased boat wakes. Increases in the frequency and intensity of boat wakes have been observed to have detrimental effects on local intertidal organisms such as the eastern oyster (*Crassostrea virginica*) (Campbell, 2015; Donnelly and Walters, 2008). The effects of boat wakes have the potential to negatively impact mangrove establishment indirectly through shoreline erosion (Balke et al., 2013; Rapaglia et al., 2011; Garel et al., 2008) or through

direct forcing if the resistance force of seedlings is low enough (Balke et al., 2011). This is especially true along much of Florida's coastline, including De Soto, where recreational and commercial boating is common. Wind-generated wakes have also been shown to erode coastal vegetated habitat (Houser, 2010) and may have increased negative effects on areas, like De Soto, that are surrounded by a large fetch. Understanding how hydrodynamic interactions impact sediment erosion around the base of seedlings is needed for future calculations of seedlings susceptibility to dislodgement. Natural mangrove failure will occur in the presence of erosion around the base of the seedling, in turn lowering its resistance force. Numerical models show the flow around a solitary mangrove seedlings taking the shape of a horseshoe vortex and eroding sediment along the front edge of the mangrove base and immediately surrounding area (Le Minor et al. 2019). These flow effects have the potential to limit the successful establishment of seedlings along restored and natural areas and impact how mangrove forests expand and regenerate. The uprooting susceptibility in the context of no erosion provided by our study begins to shed light on possible hydrodynamic limitations to recruitment and factors guiding the establishment of vegetation in these unique communities. Going forward, more focused tests on how uprooting vulnerability changes with the influence of erosion can be used to further characterize this relationship under varying levels of erosion and burial, simulating the sediment dynamics of natural mangrove forests.

While these findings show the potential for mangrove seedlings to be dislodged by hydrodynamic forces, there are still multiple unknowns that can be addressed to improve uprooting velocity estimations. There are differences in plant flexibility and morphology that we did not consider. For velocity calculations, plant flexibility was treated identically for both

mangrove species. Differences in plant flexibility should be accounted for in the future as resistance to bending is proportional to stem diameter (Boizard and Mitchell, 2011). Specific tests examining changes in flexibility as mangroves transition from propagule to seedlings would be helpful for future velocity calculations. Morphology is partially accounted for with the frontal area term in Equation 3, but differences in morphology will have effects on individual drag coefficients when measuring at the plant scale. Furthermore, mangrove seedlings were considered to be submerged vegetation for velocity calculations, wherein the entirety of its frontal area would be exposed to hydraulic flow. This may not be entirely realistic for taller seedlings that naturally extend above the local water level. However, this is partially accounted for by applying the reduction coefficient to seedlings' frontal area, allowing us to model the influence of varying seedling sizes on calculated flow velocities.

Despite these unknowns, our findings begin to provide quantifiable benchmarks that inform researchers and resource managers on what hydrodynamic environments are conducive to mangrove establishment and what physical environmental factors may be influencing successful colonization and regeneration throughout their global range. These findings help to inform on the interactions between mangrove seedlings and the hydraulic environment in order to provide a mechanistic understanding to mangrove recruitment under natural conditions, as well as provide context and direction to future research examining these complex relationships.

CHAPTER 4: CONCLUSION

Mangroves are highly diverse ecosystems that serve as some of the world's most productive environments (Kathiresan and Qasim, 2005). Current research has shown declines in much of the mangroves range, instigated by coastal development (Polidoro et al., 2010), while highlighting areas of expansion due to responses to climate change (Cavanaugh et al., 2013). Understanding how changes in the environment (e.g. increased storms, boating activity, vegetation removal) effect the successful colonization and regeneration of mangrove ecosystems is reliant on our awareness of the mechanisms guiding these processes; such knowledge is needed to predict mangrove coverage into the future.

This thesis aims to provide quantifiable limitations to establishment while identifying the effectiveness of restoration efforts in creating environments conducive to mangrove establishment. Friess et al. (2010) emphasize the need for an interdisciplinary approach to wetland ecosystem science. By incorporating both biological and physical constraints on mangrove establishment, we are better able to detect limiting factors and thresholds to mangrove regeneration and react accordingly. Going forward, future work can build on this by identifying and addressing constraints in the natural environment and improving the long-term success of restoration programs.

APPENDIX A: FIGURES

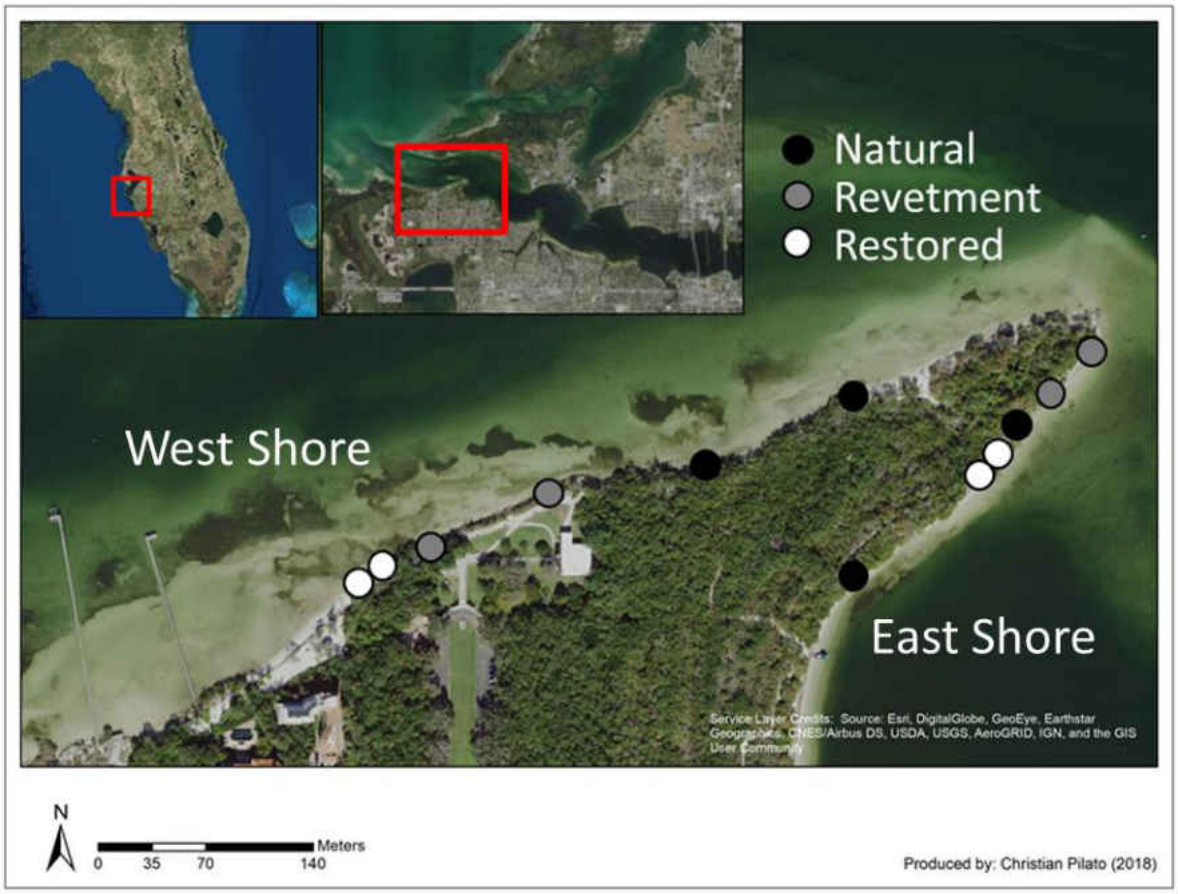

Figure 1**:** De Soto National Memorial monitoring locations.

Figure 2: Example of shoreline at De Soto National Memorial before (left) and immediately after (right) living shoreline stabilization.

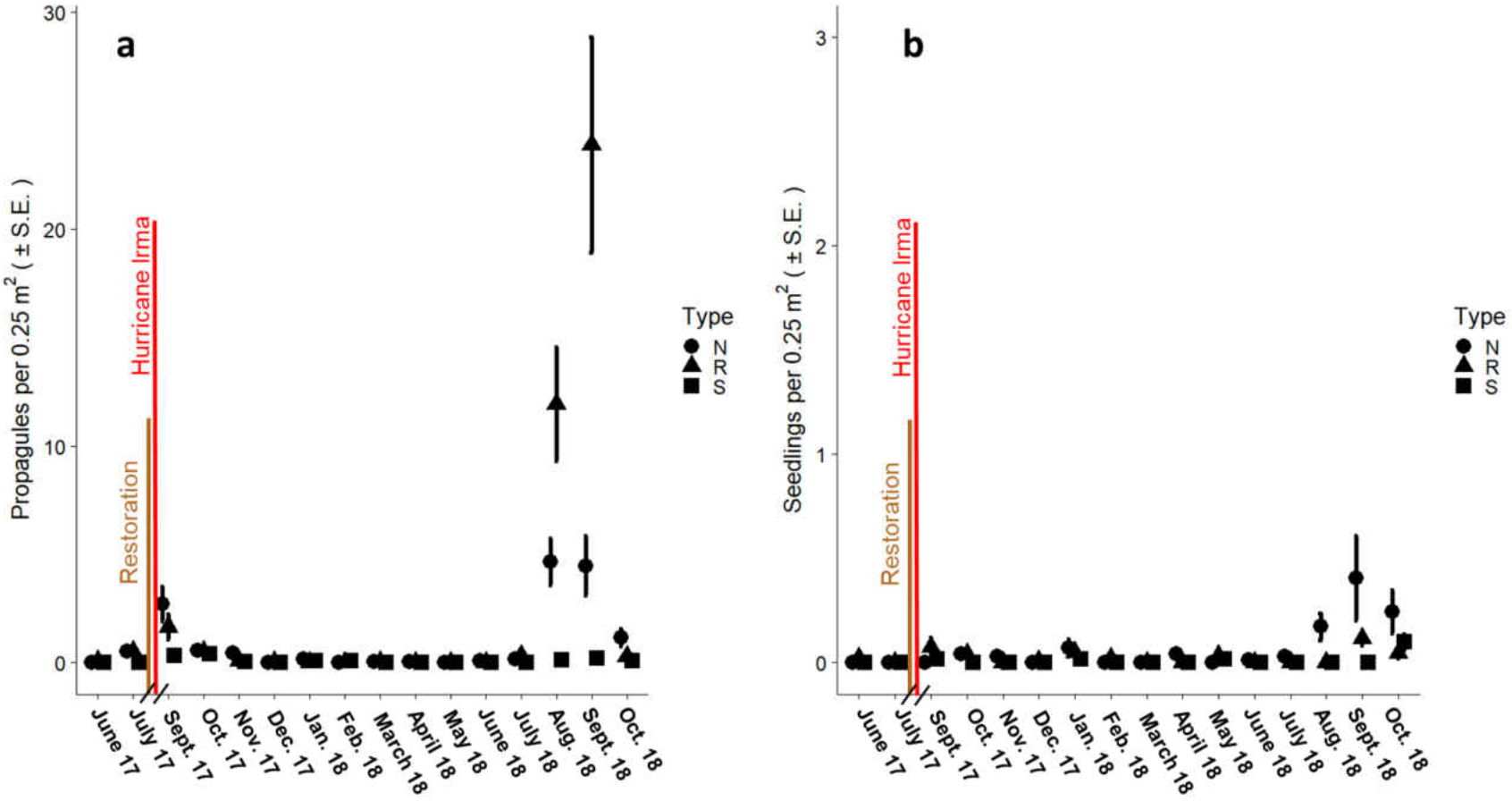

Figure 3: (a) Mean mangrove propagule count per 0.25 m^2, calculated from shoreline transects. Propagule counts were averaged across all natural (N), restored (R), and revetment (S) sites. (b) Mean number of mangrove seedlings per 0.25 m^2 calculated from shoreline transects. Seedling counts averaged across all natural (N), restored (R), and revetment (S) sites.

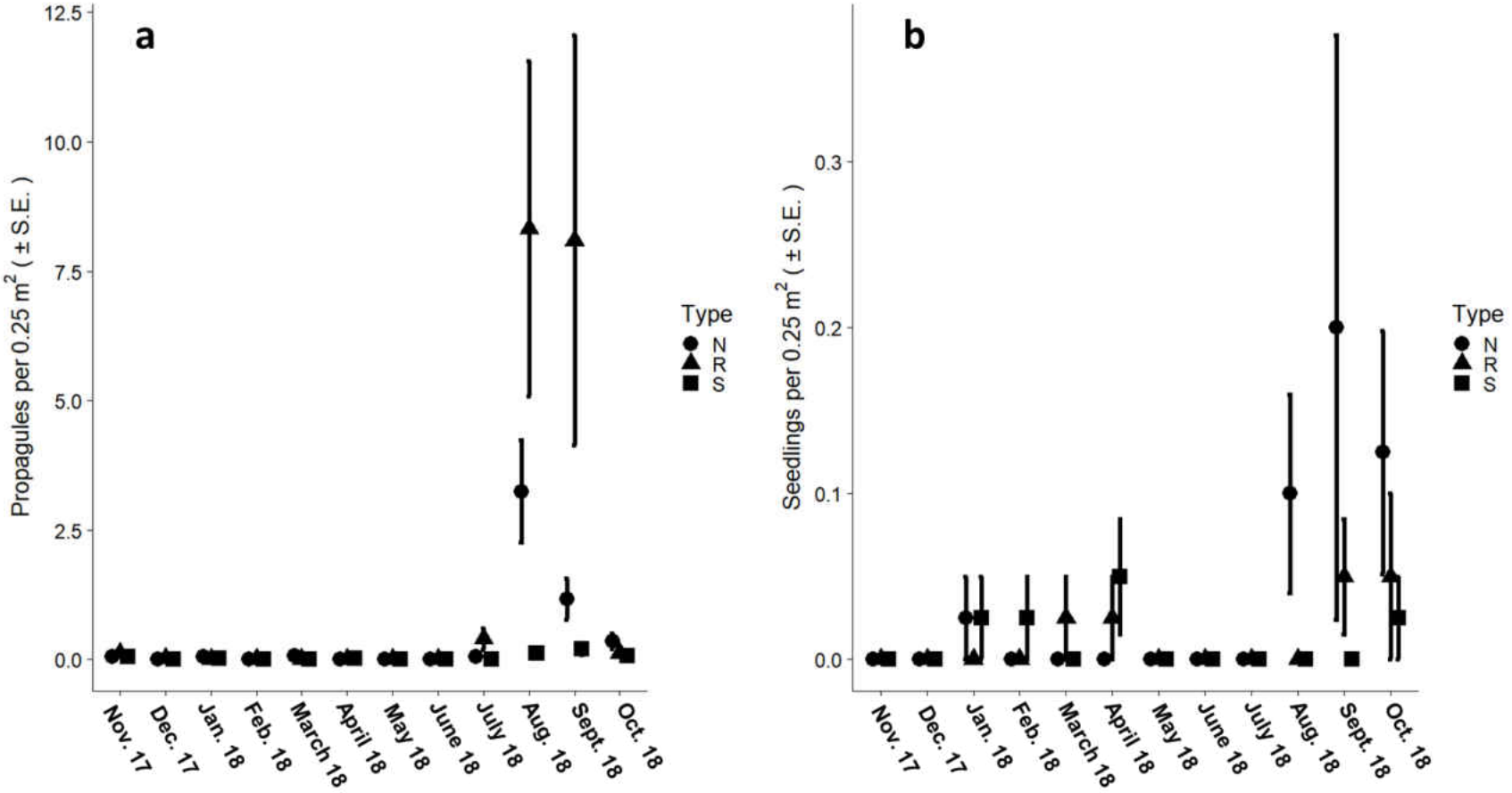

Figure 4: (a) Mean mangrove propagule count per 0.25 m^2, calculated from randomized quadrats. Propagule counts averaged across all natural (N), restored (R), and revetment (S) sites. (b) Mean mangrove seedlings per 0.25 m^2, calculated from randomized quadrats. Seedling counts averaged across all natural (N), restored (R), and revetment (S) sites.

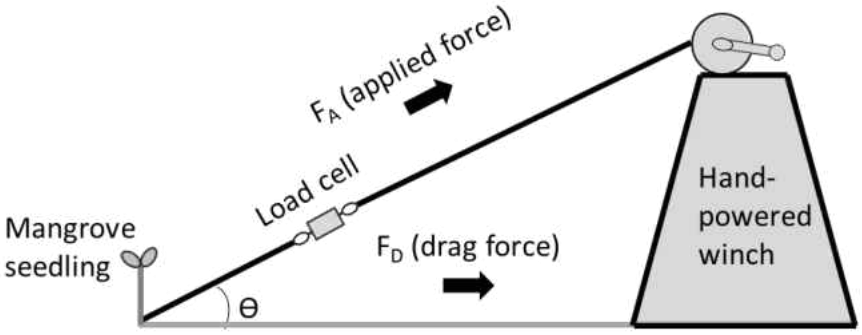

Figure 5: Lateral pull-test design. Theta (Θ) represents the angle at which mangroves were pulled.

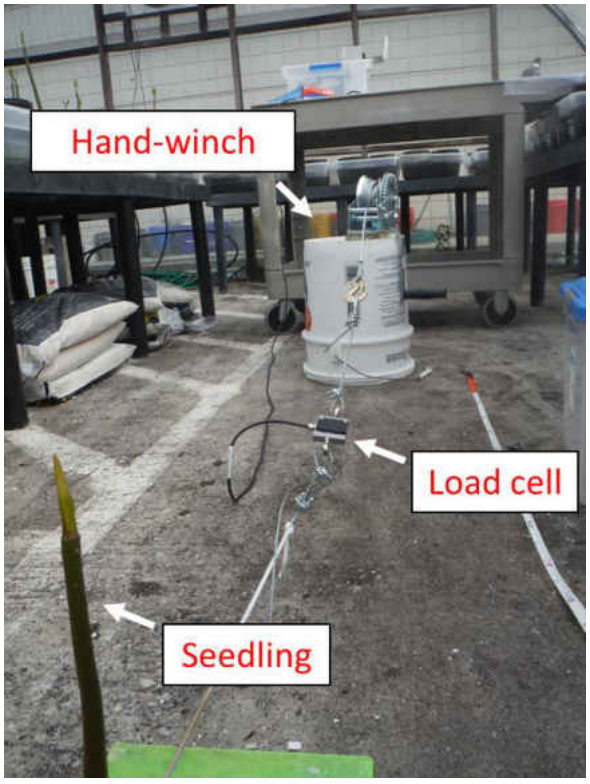

Figure 6: Lateral pull-test conducted at the University of Central Florida.

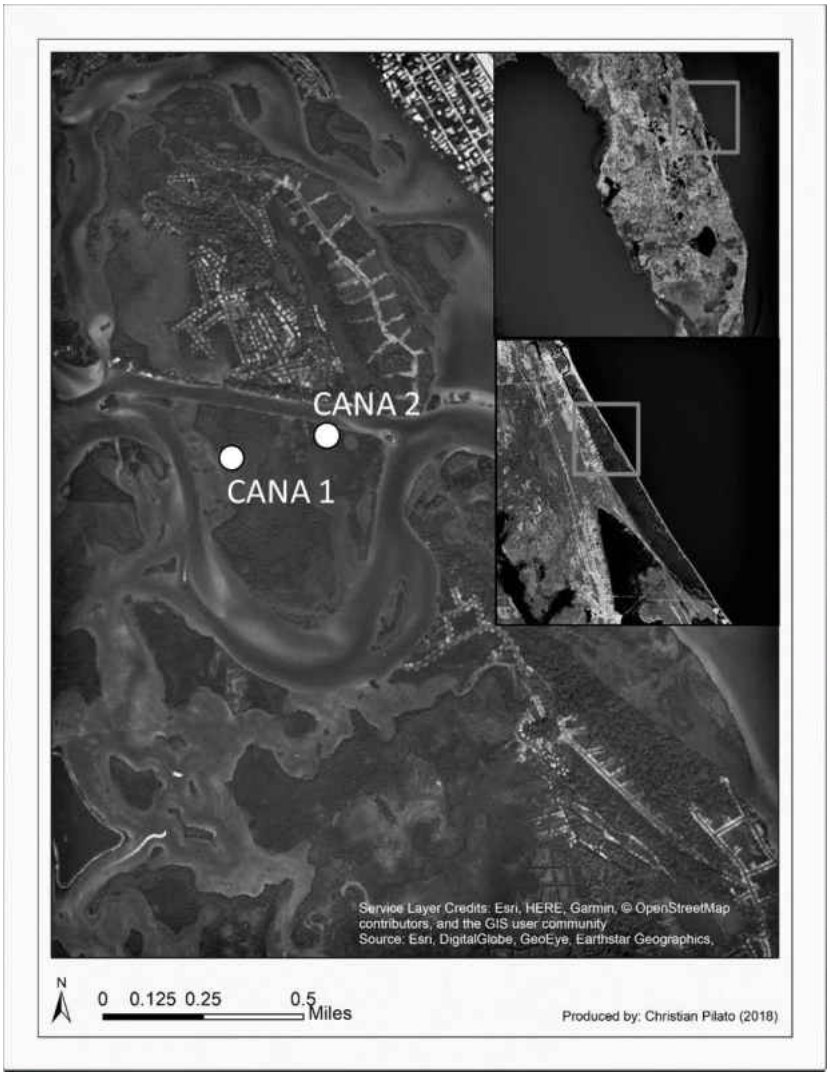

Figure 7: Pull-test locations within Canaveral National Seashore.

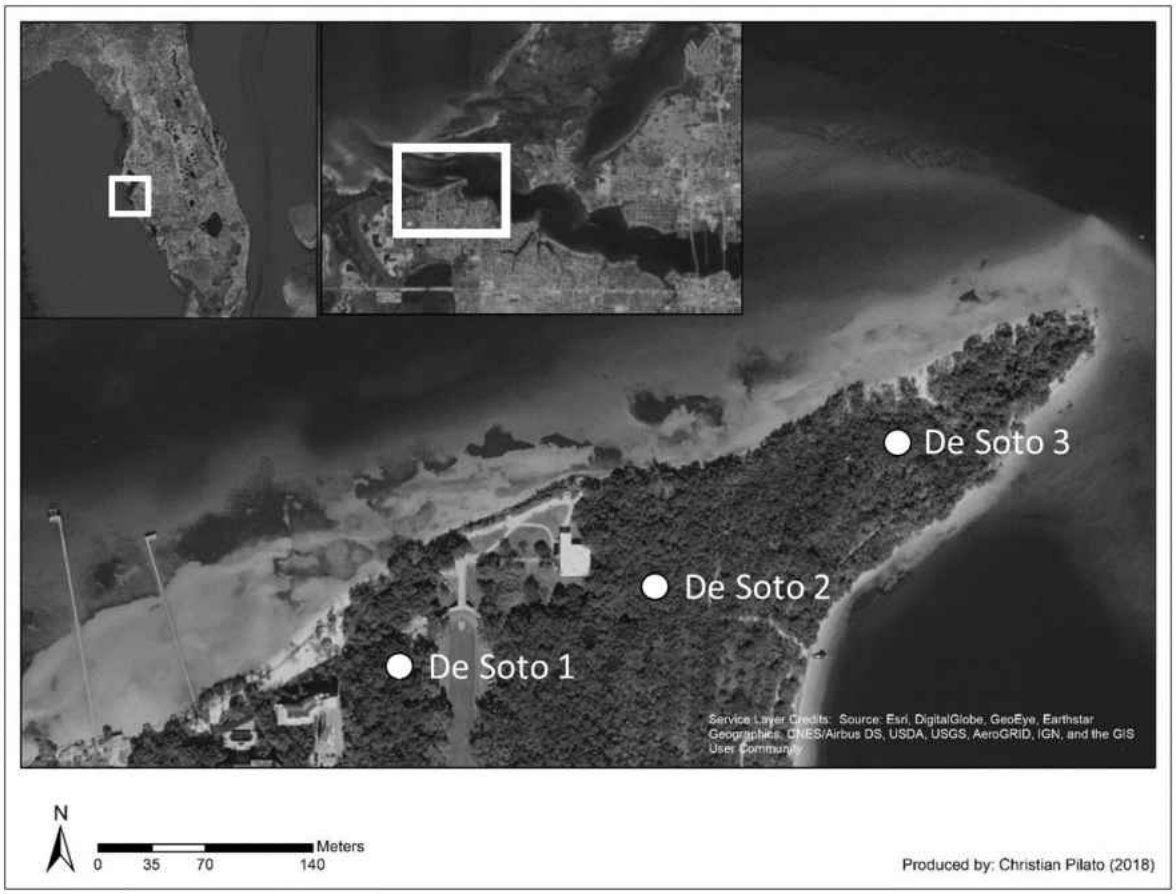

Figure 8: Pull-test locations within De Soto National Memorial.

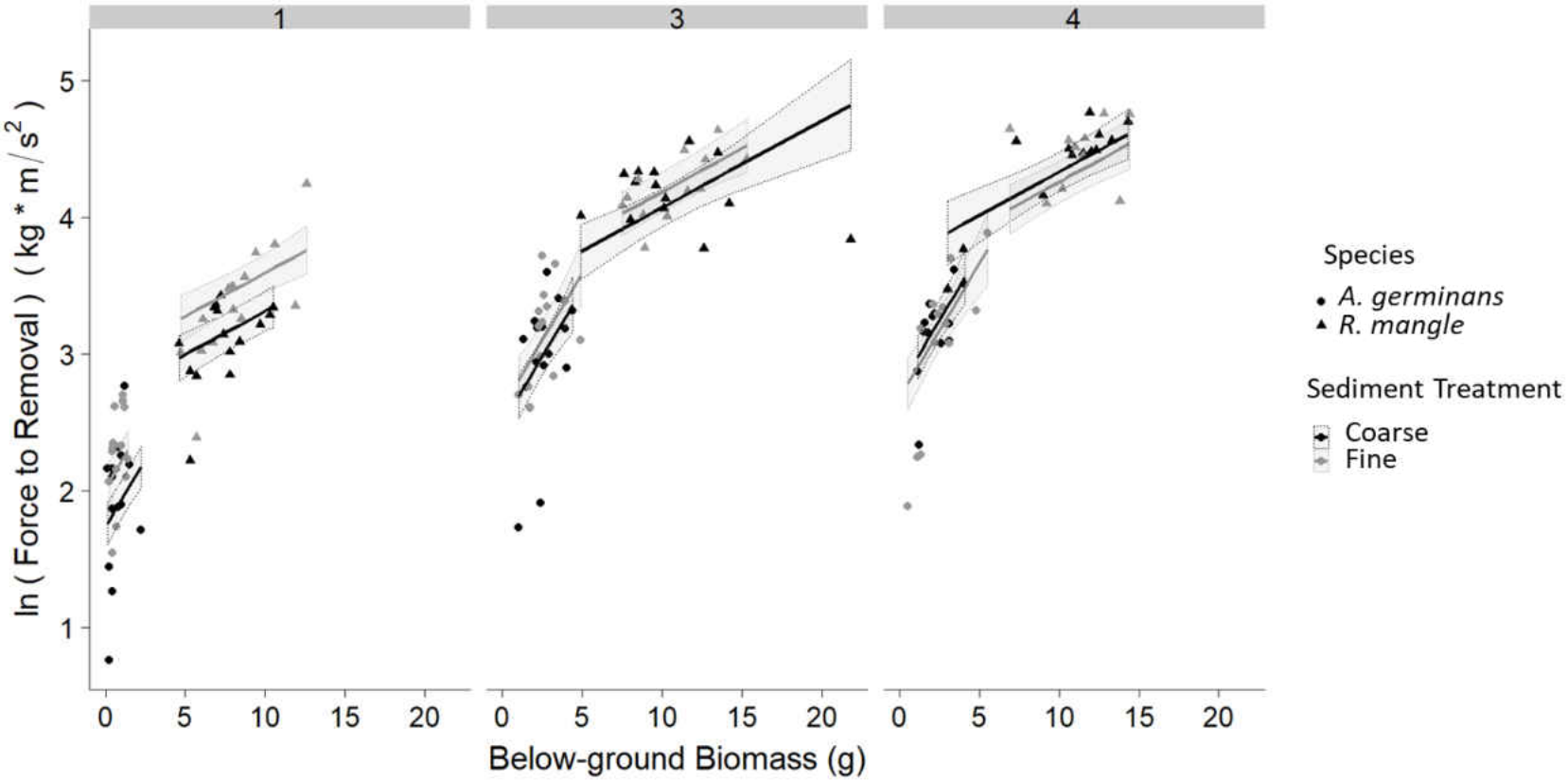

Figure 9: Linear regression model for the horizontal force to removal in greenhouse pull-tests. X-axis represents below-ground biomass. Y-axis represents the horizontal force to removal for mangrove seedlings. Different shapes represent mangrove species. Columns show 1, 3, and 4-month old seedlings. Dotted lines represent 95% confidence intervals. Y-axis is presented in natural log units.

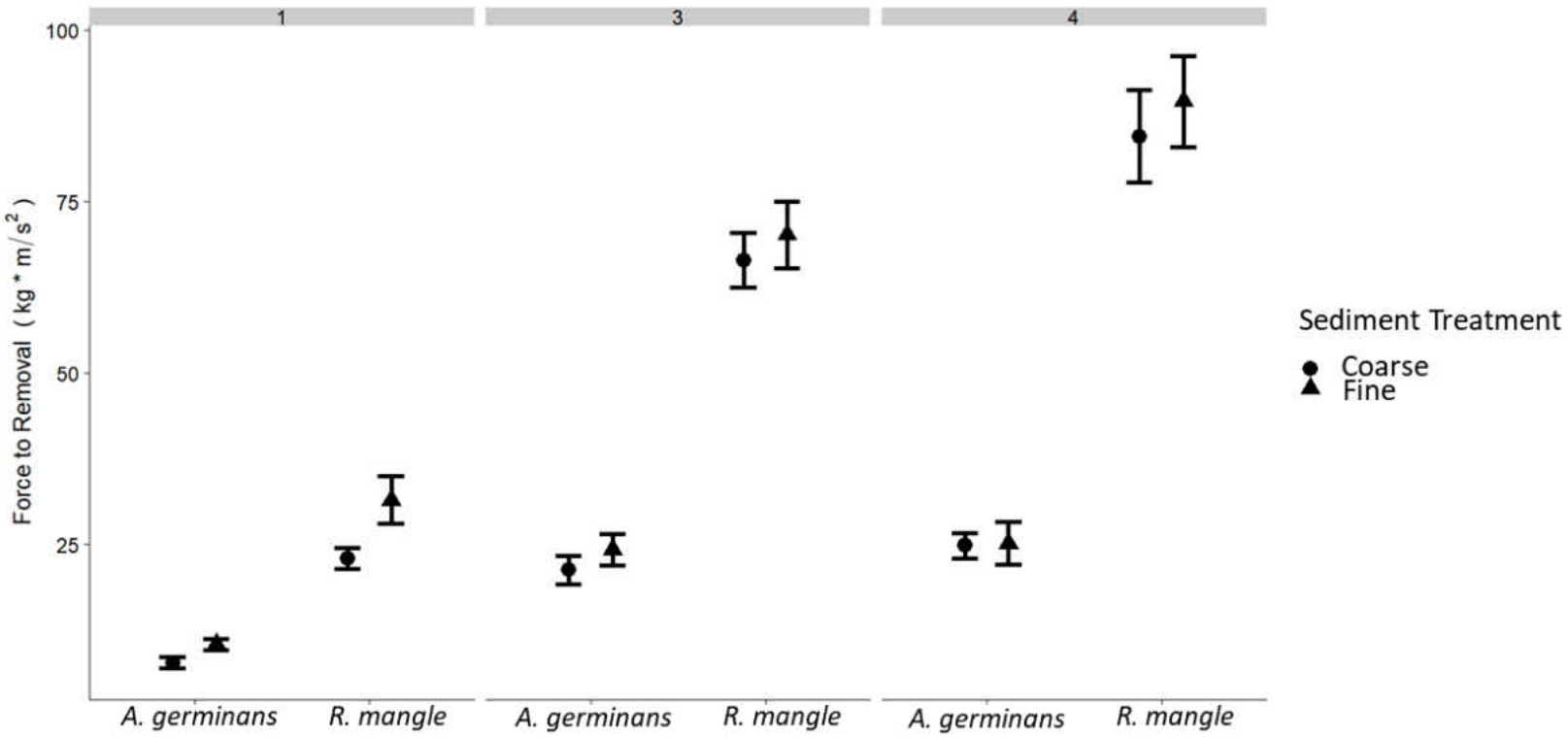

Figure 10: Mean horizontal force to removal ± S.E. of greenhouse pull-tests. Shapes represent different sediment treatments.

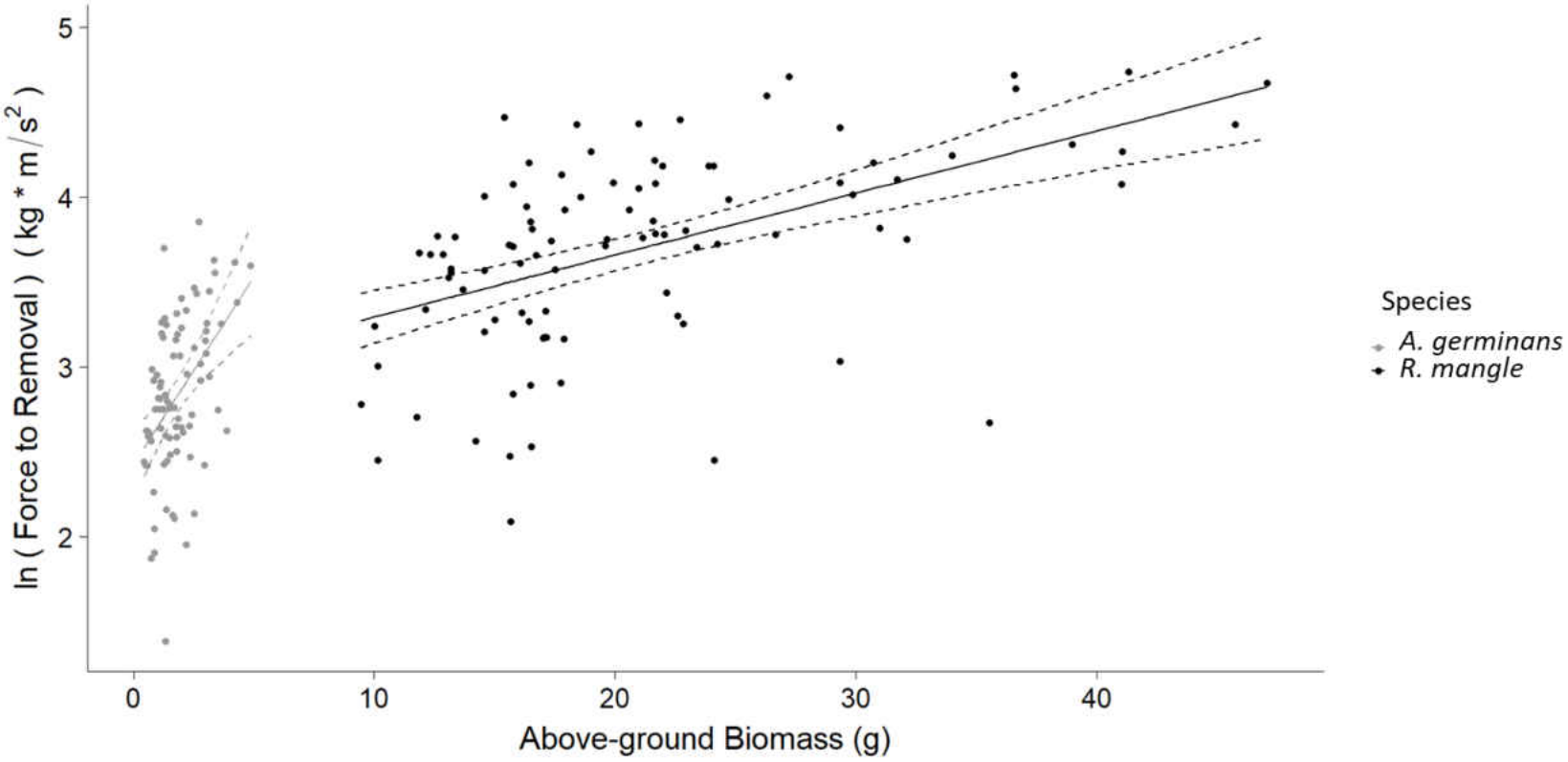

Figure 11: Linear regression model for horizontal force to removal of field pull-tests. X-axis represents above-ground biomass; Y-axis represents the horizontal force required to uproot mangrove seedlings. Different shapes represent mangrove species. Dashed lines represent the 95% confidence intervals of the model. Y-axis is presented in natural log units.

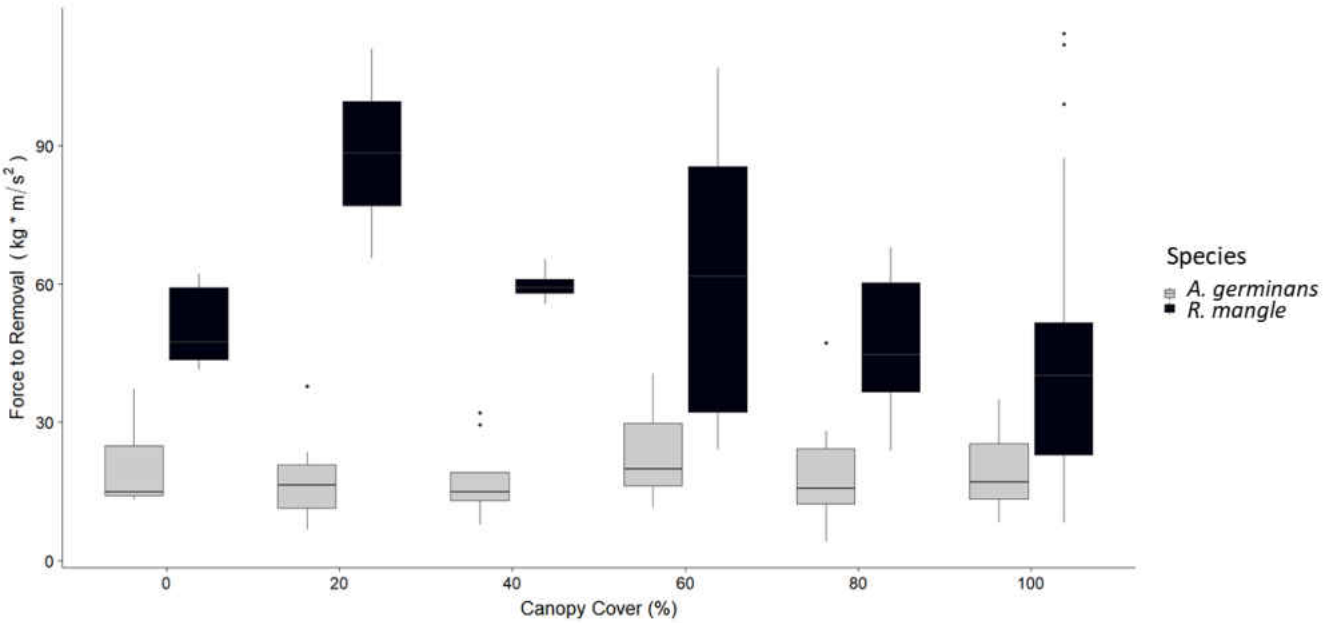

Figure 12: Mean force to removal (± S.E.) at each field site both *R. mangle* and *A. germinans*.

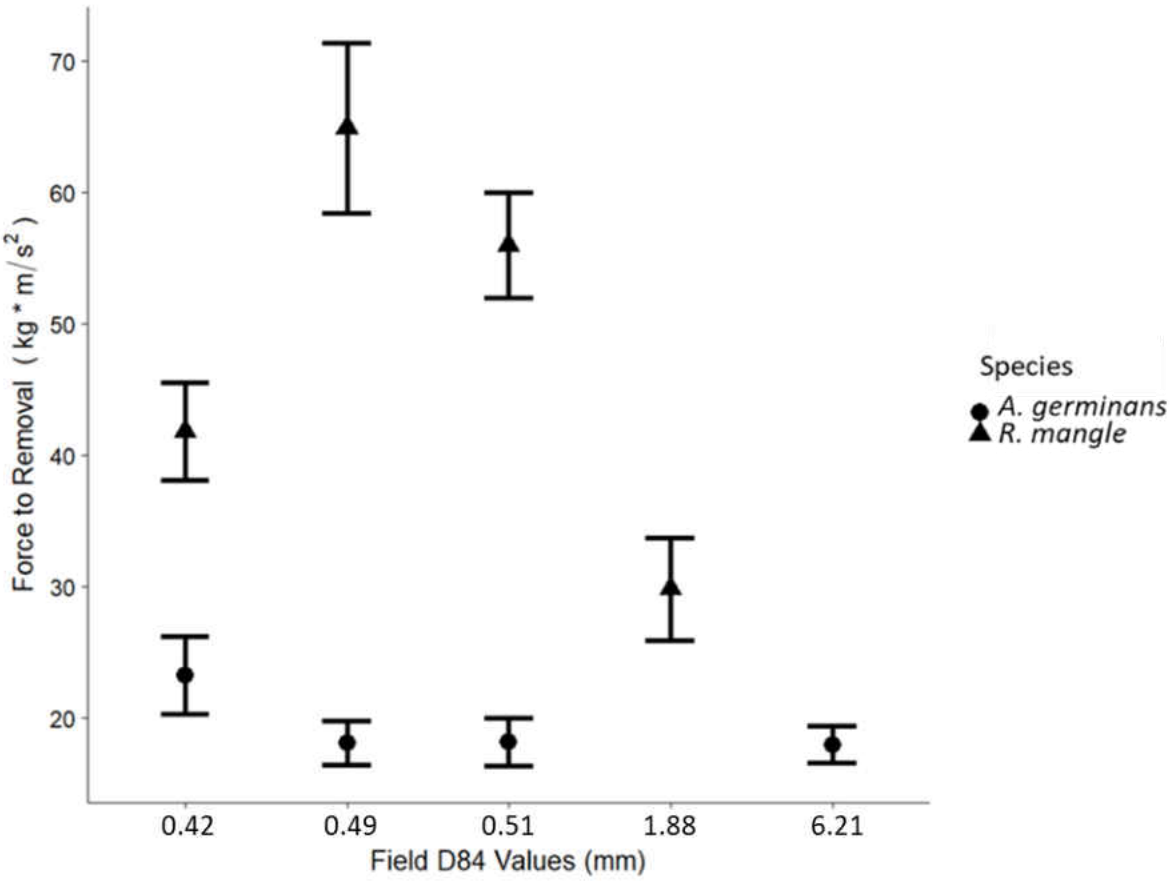

Figure 13: Mean force to removal (± S.E.) across field sediment grain sizes characterized by D84 values. Each grain size on X-axis represents sediment characterized at individual sites.

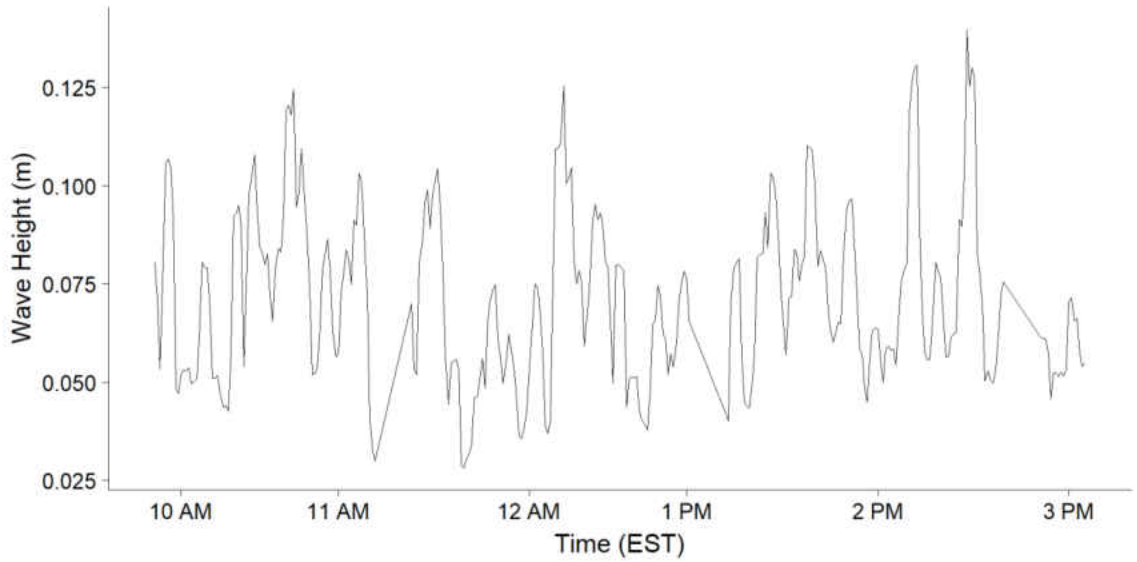

Figure 14: Significant wave heights measured on July 2, 2018 at De Soto National Memorial.

APPENDIX B: TABLES

Table 1: Mean groundcover values across sample locations. Values averaged across all 4 sites of each shoreline type from 16 months of surveys.

	% Sand	% Shell	% Vegetation	% Cement/Natural Rock	% Driftwood
Restored	64.4 ± 0.9	24.1 ± 0.8	2.7 ± 0.2	8.3 ± 0.6	0.3 ± 0.0
Revetment	33.1 ± 1.2	16.5 ± 0.9	2.8 ± 0.5	47.6 ± 1.4	0.0 ± 0.0
Natural	49.2 ± 1.1	31.9 ± 1.0	8.7 ± 0.6	9.2 ± 0.7	0.9 ± 0.1

Table 2: AICc table of top 4 models predicting total propagule count along shoreline transects (totalAprop) as a function of shoreline type (restored, natural, revetment), month surveyed, and percent cover of surrounding vegetation (Perc.Veg), and location within the park (West/East shore).

#	Model	AICc	Δ AICc	weight
2	totalAprop~ Type + Month + Perc.Veg + Location	240.4	0	0.7829
1	totalAprop ~ Type + Month + Location	243.0	2.6	0.2111
6	totalAprop~ Type + Month + Perc.Veg	251.0	9.8	0.0059
8	totalAprop ~ Type + Month	259.0	18.7	<0.001

Table 3: Parameter estimates for negative binomial generalized linear model predicting propagule abundance as a function of shoreline type, month surveyed, surrounding vegetation (Perc.Veg), and locations within the park (West/East shore) for shoreline transect surveys. Shoreline type includes restored, natural, and revetment levels. Month variable includes months from 2017 and 2018 propagule seasons. Coefficients are based on the "restored" shoreline type, July '17, and East set as the reference level.

	Estimates	Std. Error	z value	Pr(>|z|)
Intercept	-1.4151	0.5815	-2.434	0.0150
Natural	-0.8883	0.3433	-2.588	0.0100
Revetment	-3.0164	0.5622	-5.366	<0.001
September'17	1.0759	0.6266	1.717	0.0860
October'17	0.2070	0.7128	0.290	0.7715
November'17	-1.1038	0.9298	-1.187	0.2352
July'18	-0.2739	0.7878	-0.348	0.7281
August'18	2.4814	0.5866	4.230	<0.001
September'18	2.7437	0.5803	4.728	<0.001
October'18	0.0678	0.7271	0.093	0.9258
Perc.Veg	0.0502	0.0209	2.400	0.0164
West shore	1.4017	0.3353	4.180	<0.001

Table 4: AICc table of top 4 models predicting total propagule count within randomized quadrats (totalAprop) as a function of month surveyed, shoreline type (restored, natural, revetment), and percent cover of surrounding vegetation (Perc.Veg).

#	Model	AICc	Δ AICc	weight
7	totalAprop~ Type + Month + Location	924.6	0	0.677
8	totalAprop~ Type + Month + Perc.Veg + Location	926.5	1.9	0.266
5	totalAprop~ Type + Month	930.2	5.6	0.042
3	totalAprop ~ Type + Month + Perc.Veg	932.2	7.6	0.015

Table 5: Parameter estimates for the negative binomial generalized linear model (model 7) predicting propagule abundance as a function of shoreline type and month surveyed for randomized quadrat surveys. Shoreline type includes restored, natural, and revetment levels. Month variable includes 2018 propagule seasons. Coefficients are based on the "restored" shoreline type, July'18, and East set as the reference level.

	Estimates	Std. Error	z value	Pr(>|z|)
Intercept	-1.3634	0.4117	-3.312	<0.001
Natural	-1.0614	0.3089	-3.436	<0.001
Revetment	-3.4308	0.4111	-8.344	<0.001
August '18	2.9102	0.4370	6.659	<0.001
September '18	2.4035	0.4400	5.463	<0.001
October '18	0.3643	0.4793	0.760	0.447
West shore	0.8657	0.2826	3.099	0.002

Table 6: Mean summary statistics (± S.E.) for seedlings tested in greenhouse lateral pull-tests.

Species	Age (months)	Above-ground Biomass (g)	Below-ground Biomass (g)	Height (cm)
A. germinans	1	2.7 ± 0.2	0.8 ± 0.1	9.5 ± 0.5
R. mangle	1	16.0 ± 0.7	7.8 ± 0.4	25.2 ± 0.9
A. germinans	3	2.4 ± 0.2	2.6 ± 0.2	15.2 ± 0.6
R. mangle	3	19.3 ± 0.7	10.7 ± 0.7	31.8 ± 0.9
A. germinans	4	2.6 ± 0.3	2.4 ± 0.2	15.2 ± 0.8
R. mangle	4	18.3 ± 1.2	10.6 ± 0.6	31.2 ± 1.4

Table 7: Mean summary statistics (± S.E.) for seedlings tested with in-field lateral pull-tests.

Canaveral National Seashore					
Species	**Above-ground Biomass (g)**	**Below-ground Biomass (g)**	**Height (cm)**	**Leaf Number**	**Basal Diameter (cm)**
A. germinans	2.1 ± 0.1	0.6 ± 0.0	21.8 ± 0.6	4.7 ± 0.2	0.4 ± 0.0
R. mangle	24.9 ± 1.4	6.4 ± 0.4	42.8 ± 1.3	7.5 ± 0.5	1.2 ± 0.0

De Soto National Memorial					
Species	**Above-ground Biomass (g)**	**Below-ground Biomass (g)**	**Height (cm)**	**Leaf Number**	**Basal Diameter (cm)**
A. germinans	1.4 ± 0.2	0.7 ± 0.1	19.7 ± 0.9	4.5 ± 0.3	0.3 ± 0.0
R. mangle	17.7 ± 0.8	6.6 ± 0.4	35.5 ± 0.9	5.1 ± 0.3	1.2 ± 0.0

Table 8: AIC table of top 4 models predicting changes in the horizontal force to removal (Horiz..Force..N.) as a function of below-ground biomass (BG.Biomass), species (Sp.), age, and sediment treatment (sed) for greenhouse pull-tests.

#	**Model**	**AICc**	**Δ AICc**	**weight**
9	log(Horiz..Force..N.) ~ BG.Biomass * Sp. + sed * Age	126.1	0	0.823
10	log(Horiz..Force..N.) ~ BG.Biomass * Sp. + sed + Age	129.6	3.5	0.142
3	log(Horiz..Force..N.) ~ BG.Biomass * Sp. + Age	132.5	6.4	0.034
8	log(Horiz..Force..N.) ~ BG.Biomass + Sp. + sed + Age	140.5	14.4	<0.001

Table 9: Parameter estimates for linear model (model 9) predicting the change in log(horizontal force to removal) as a function of below-ground Biomass (BG.Biomass), species, sediment treatment, and age (months) for greenhouse pull-tests. Coefficients are based on 1 month *A. germinans* in the coarse sediment treatment set as the reference level.

	Estimates	**Std. Error**	**t value**	**Pr(>|t|)**
Intercept	1.74262	0.07502	24.346	<0.001
BG.Biomass	0.19579	0.03580	5.352	<0.001
R. mangle	0.93614	0.14639	6.388	<0.001
Fine	0.28001	0.05431	2.178	0.0309
3 months	0.75687	0.07717	8.796	<0.001
4 months	1.01866	0.07727	10.993	<0.001
BG.Biomass:R. mangle	-0.13226	0.03578	-3.585	<0.001
Fine:3 months	-0.16509	0.12749	-1.295	0.197
Fine:4 months	-0.35429	0.13143	-2.696	0.008

Table 10: Summary parameters for field sediment samples through wet/dry sieving and loss on ignition tests. D84/50 were derived from the combined results of the wet and dry sieve analysis. Fraction less than 0.075mm was determined through wet sieving through a 0.075mm sieve. Percent organic matter values were derived from loss on ignition tests.

	D84 (mm)	D50 (mm)	% <0.075mm	% Organic Matter
CANA 1	0.51	0.22	28.5	29.7
CANA 2	0.49	0.21	14.2	16
De Soto 1	1.88	0.32	5.4	28.5
De Soto 2	6.21	0.46	21.5	56.4
De Soto 3	0.42	0.22	6.2	10.4

Table 11: AIC table of top 4 models predicting changes in the horizontal force to removal (Horiz..Force..N.) as a function of above-ground biomass (AG.Biomass), species (Sp.), Park, percent cover of surrounding vegetation (Perc.Veg), and percent canopy cover (Perc.Canopy) for field pull-tests.

#	Model	AICc	Δ AICc	weight
4	log(Horiz..Force..N.) ~ AG.Biomass * Sp.	241.8	0	0.556
6	log(Horiz..Force..N.) ~ AG.Biomass * Sp.+ Park	243.5	1.7	0.239
7	log(Horiz..Force..N.)~ AG.Biomass * Sp. + Perc.Canopy	243.8	2.0	0.200
3	log(Horiz..Force..N.) ~ AG.Biomass	251.2	9.4	0.005

Table 12: Parameter estimates for linear model (model 4) predicting the change in log(horizontal force to removal) as a function of above-ground biomass (AG.Biomass) and species (Sp.) Coefficients are based on *A. germinans* set as the reference level.

	Estimates	Std. Error	t value	Pr(>|t|)
Intercept	2.42691	0.10529	23.070	<0.001
AG.Biomass	0.22031	0.05075	4.341	<0.001
R. mangle	0.50066	0.16675	3.002	0.0031
AG.Biomass:R. mangle	-0.18381	0.05107	-3.599	<0.001

APPENDIX C: SUPPLEMENTARY MATERIALS

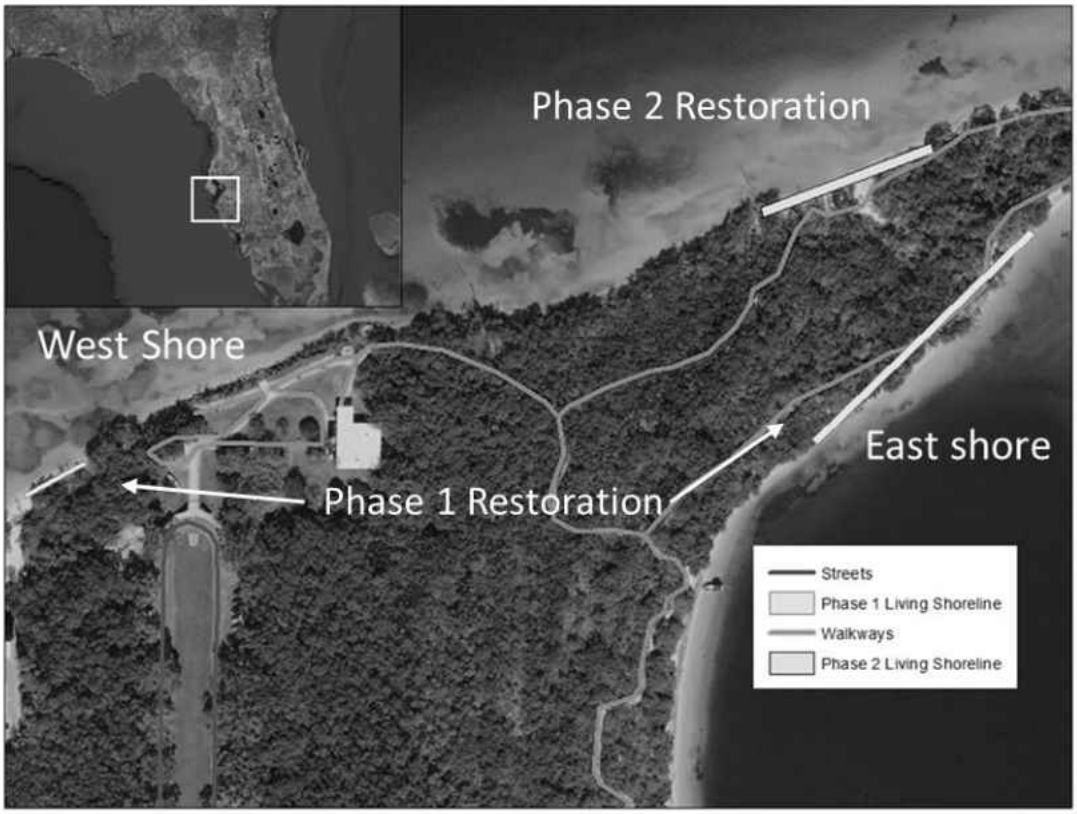

Figure 15: Living shoreline locations within De Soto National Memorial.

Figure 16: Percent survival of mangroves across both west and east living shoreline sites. Increase in *R. mangle* survival at month 6 is due to replanting mangroves to compensate for losses caused by Hurricane Irma. Hurricane Irma occurred in between months 0.5 and 1.

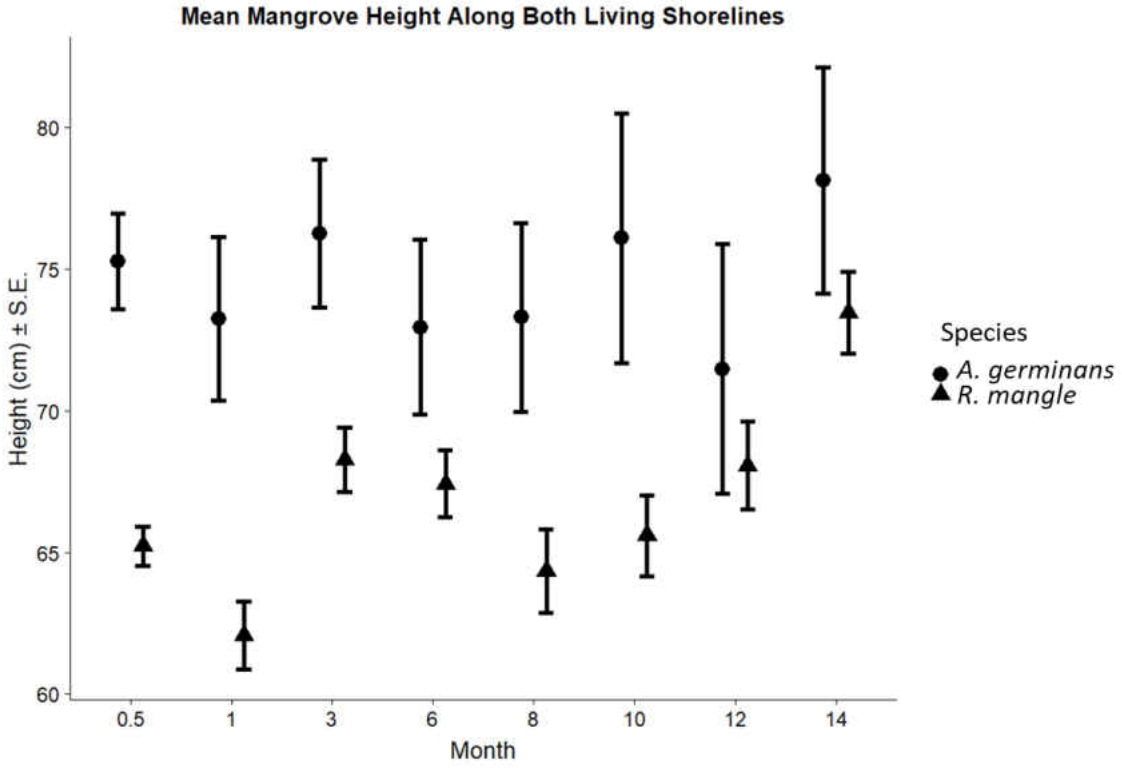

Figure 17: Mean height for planted mangroves at west and east living shoreline sites within De Soto National Memorial.

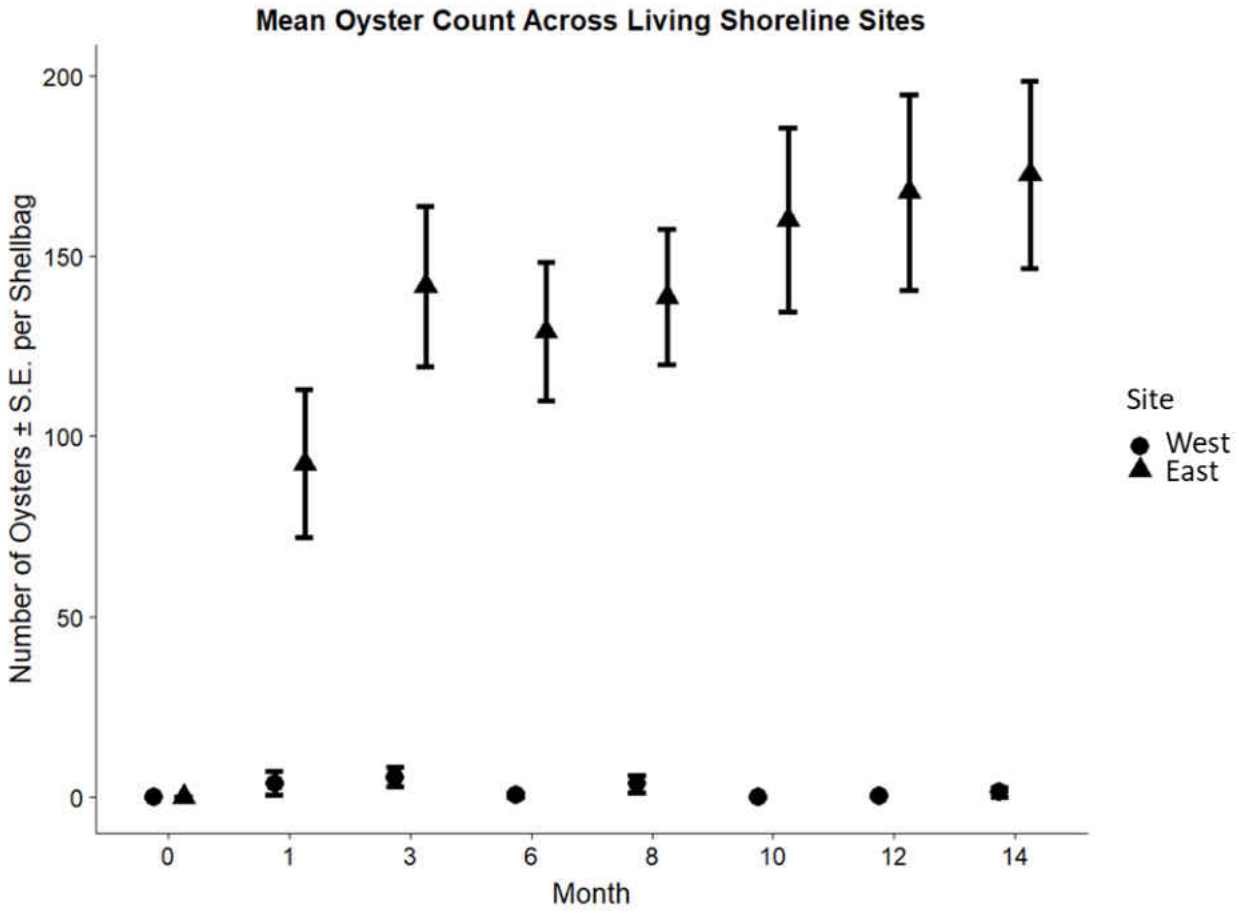

Figure 18: Mean oyster recruitment per shellbag across both west and east living shoreline sites within De Soto National Memorial.

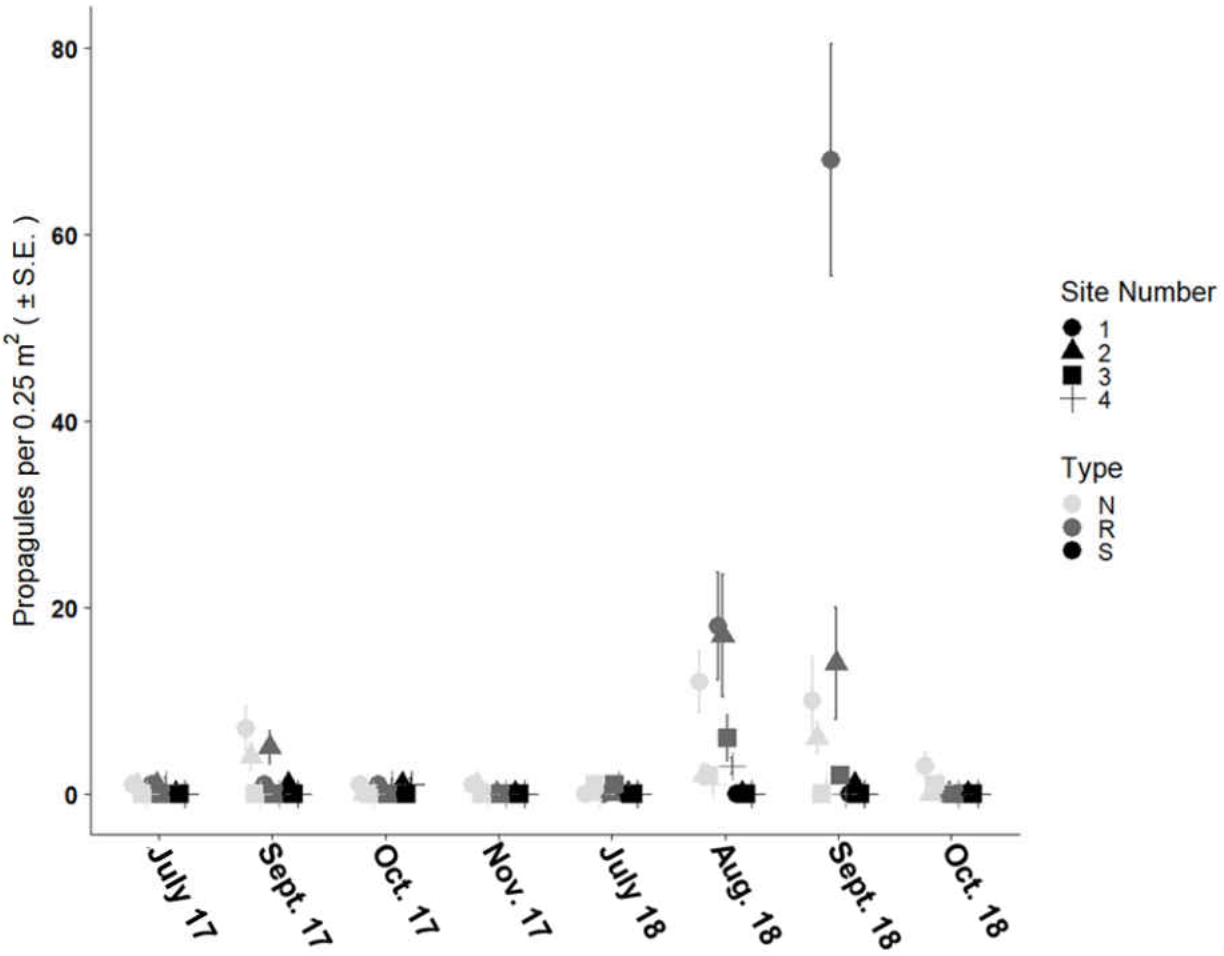

Figure 19: Mean propagule count per 0.25 m^2 quadrat for shoreline transect surveys grouped by survey site (1-4) and shoreline type: natural (N), restored (R), and revetment (S) for 2017 and 2018 propagule seasons.

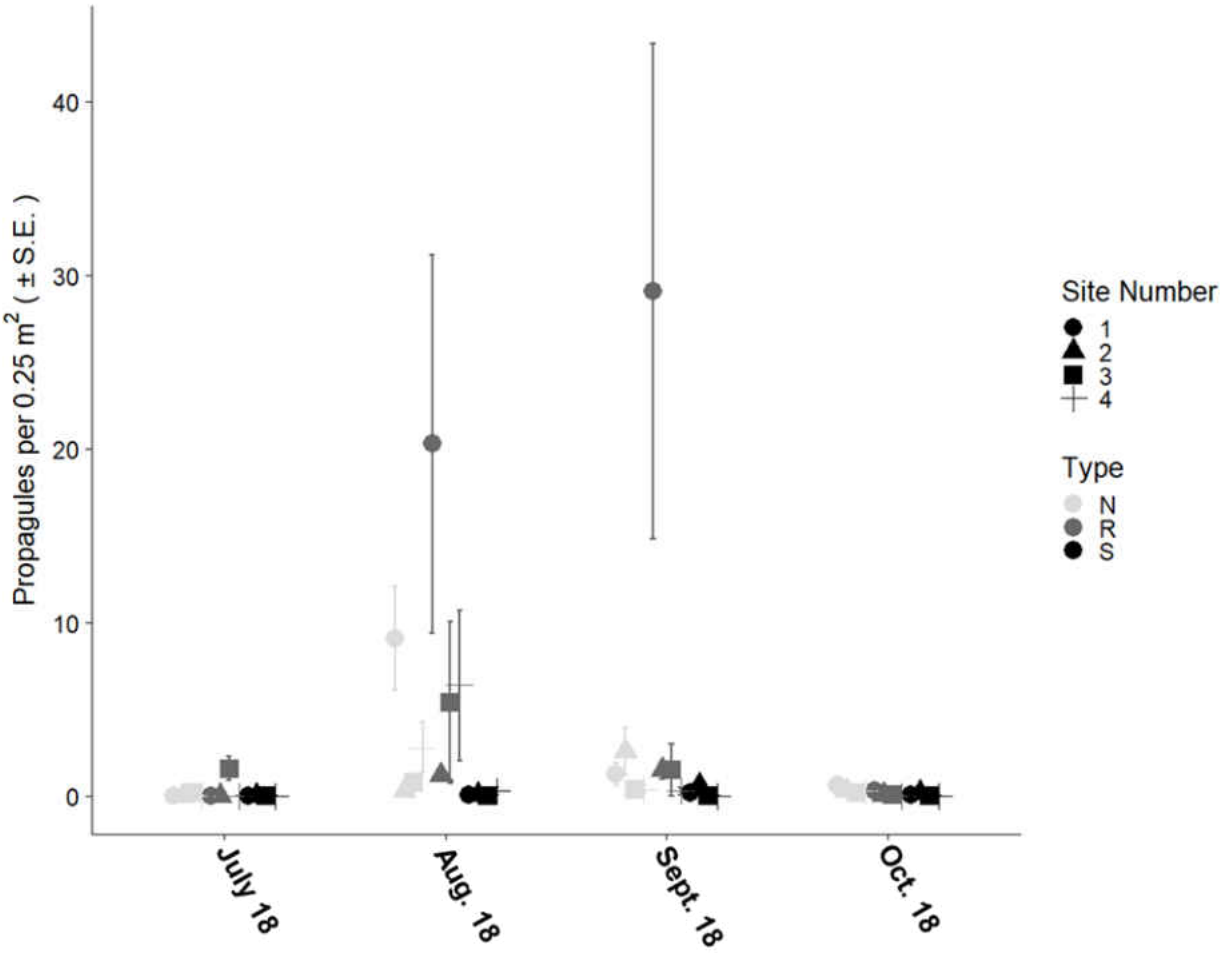

Figure 20: Mean propagule count per 0.25 m^2 quadrat for randomized quadrat surveys grouped by survey site (1-4) and shoreline type: natural (N), restored (R), and revetment (S) for 2018 propagule season.

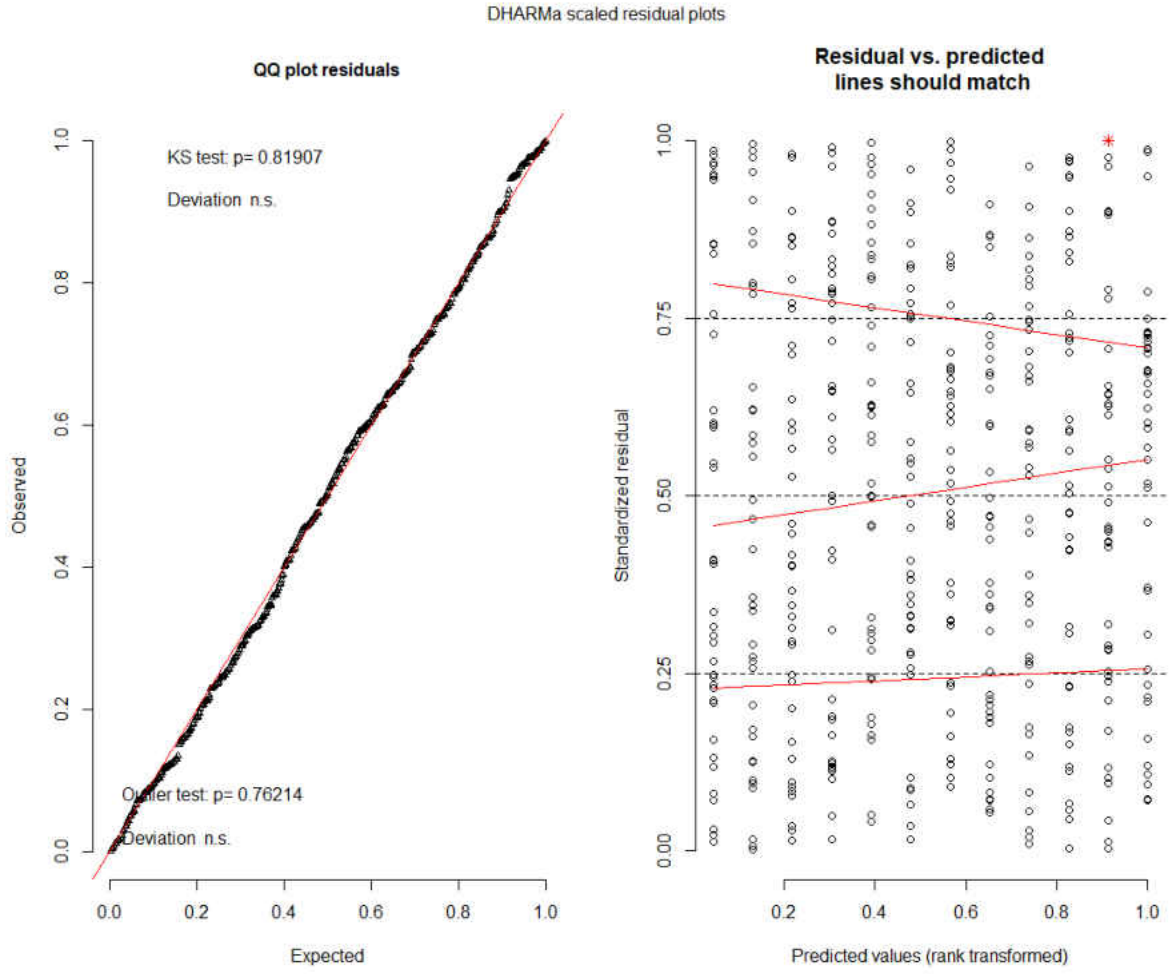

Figure 21: Simulated scaled residuals from negative binomial generalized linear model predicting propagule abundance as a function of month surveyed and shoreline type for the randomized quadrat propagule survey. (Left) Plot showing no significant deviations from the expected distribution. (Right) Plot showing a slight bias in the residuals but no significant signs of over/underdispersion.

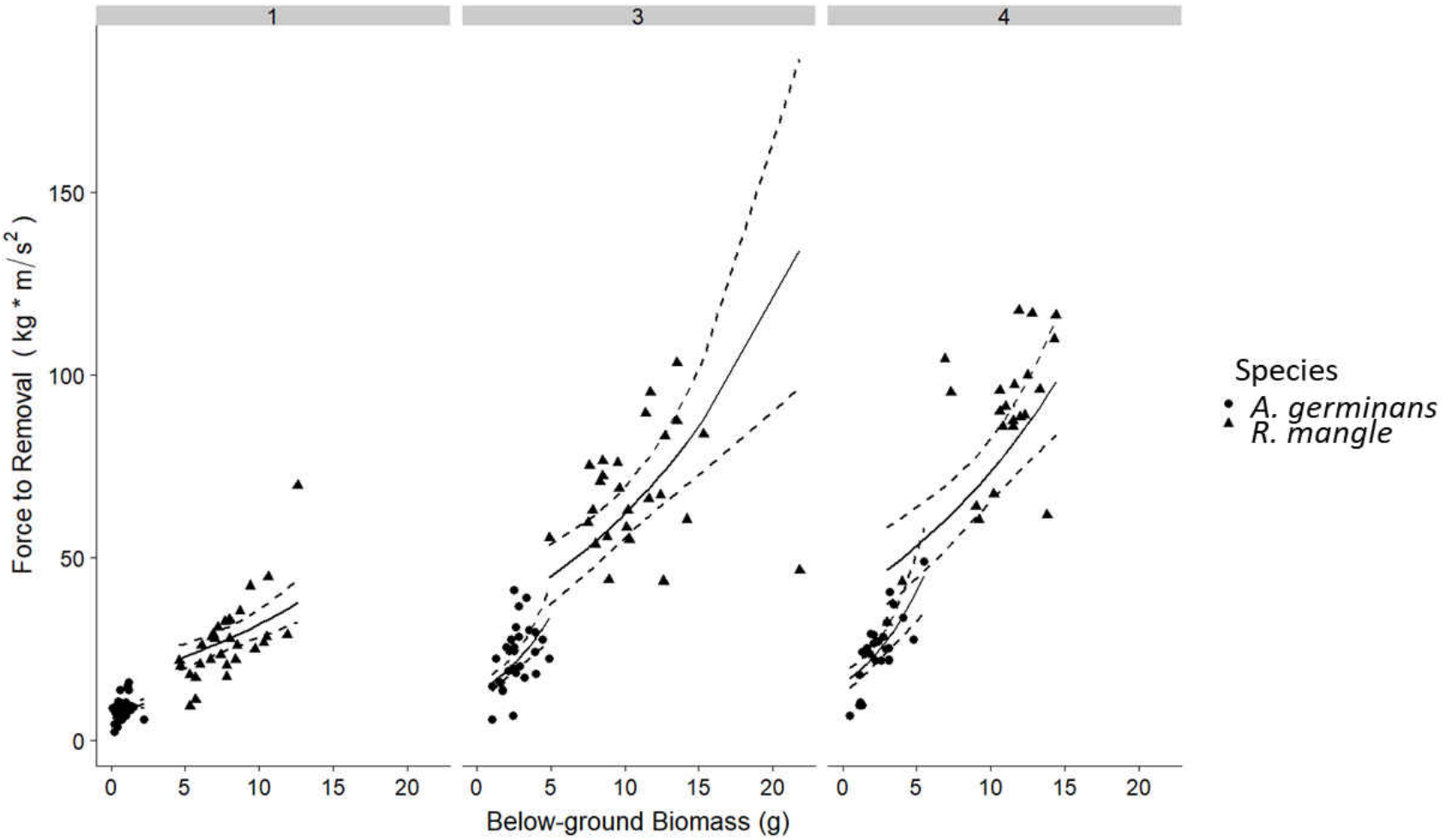

Figure 22: Linear regression model for the horizontal force to removal of greenhouse pull-tests. X-axis represents below-ground biomass. Y-axis represents the horizontal force to removal for mangrove seedlings. Different shapes represent mangrove species. Columns show 1, 3, and 4-month old seedlings. Dotted lines represent 95% confidence intervals.

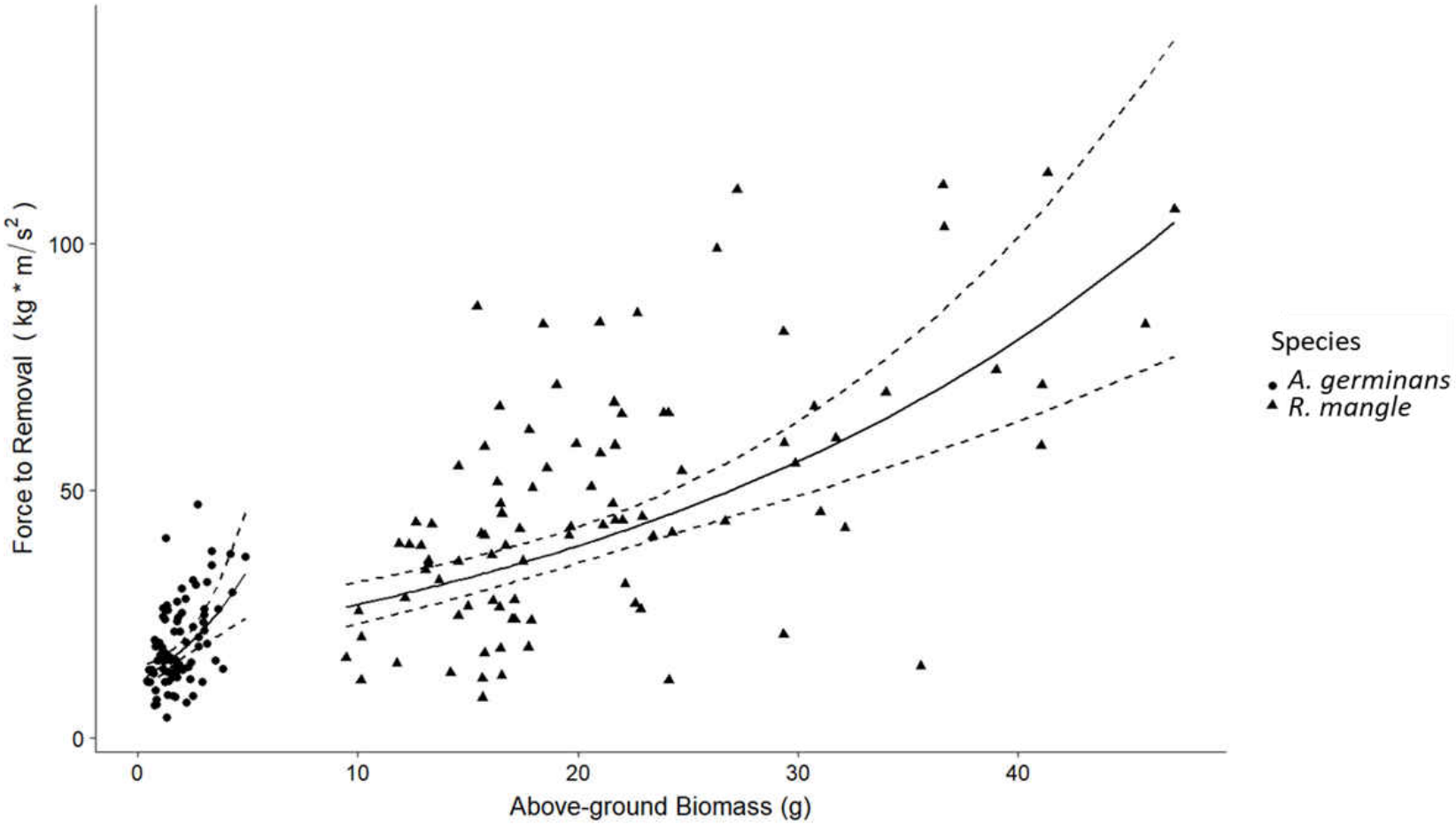

Figure 23: Linear regression model for horizontal force to removal of field pull-tests. Model predictions were back-transformed and presented in natural units. X-axis represents above-ground biomass; Y-axis represents the horizontal force required to uproot mangrove seedlings. Different shapes represent mangrove species. Dashed lines represent the 95% confidence intervals of the model.

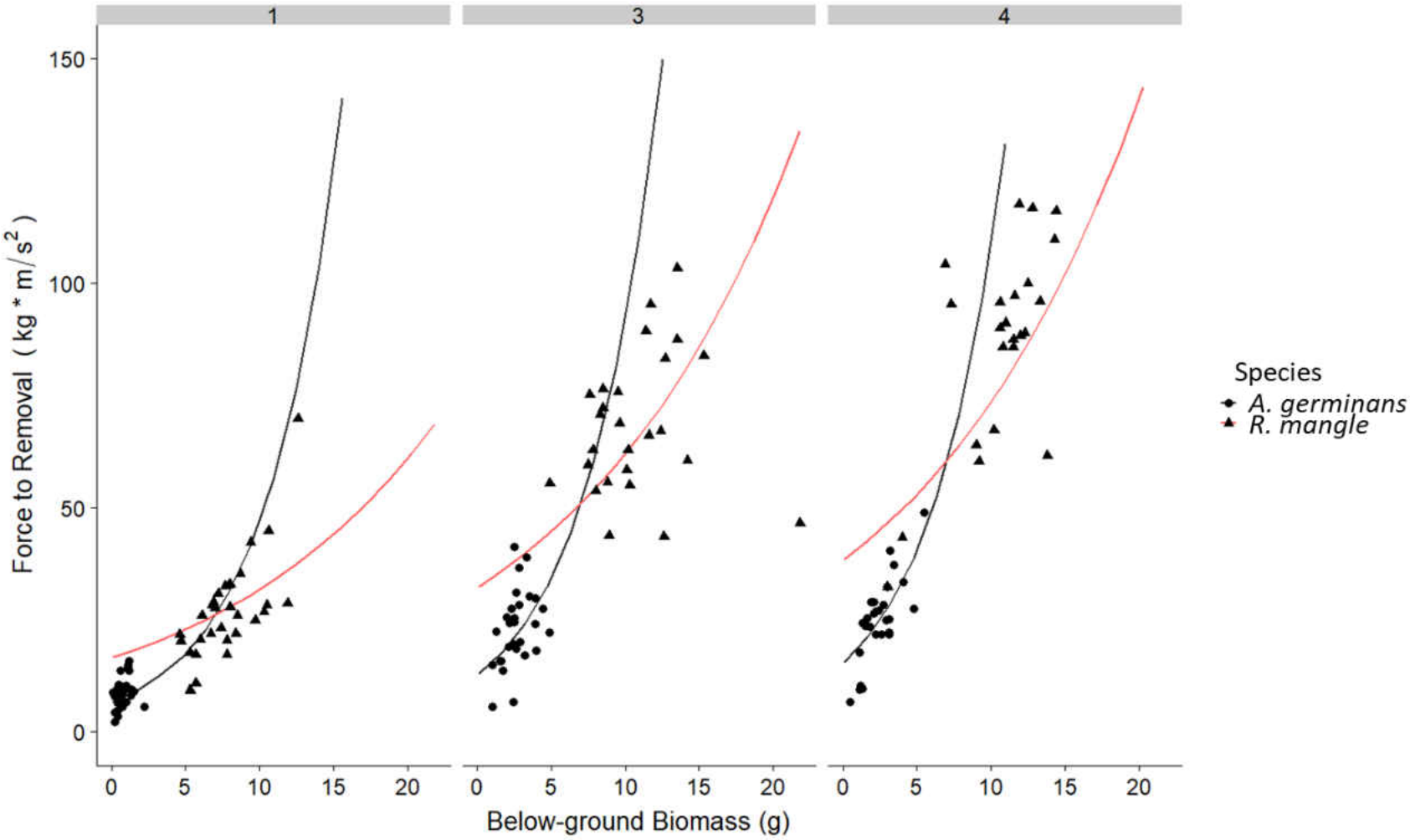

Figure 24: Model predictions for top performing model showing horizontal force to removal as a function of below-ground biomass, species, and age for greenhouse pull-tests. Model predictions were made by simulating new below-ground biomass data to generate force to removal predictions for seedlings with equivalent biomass. The overlaid points represent the observed data

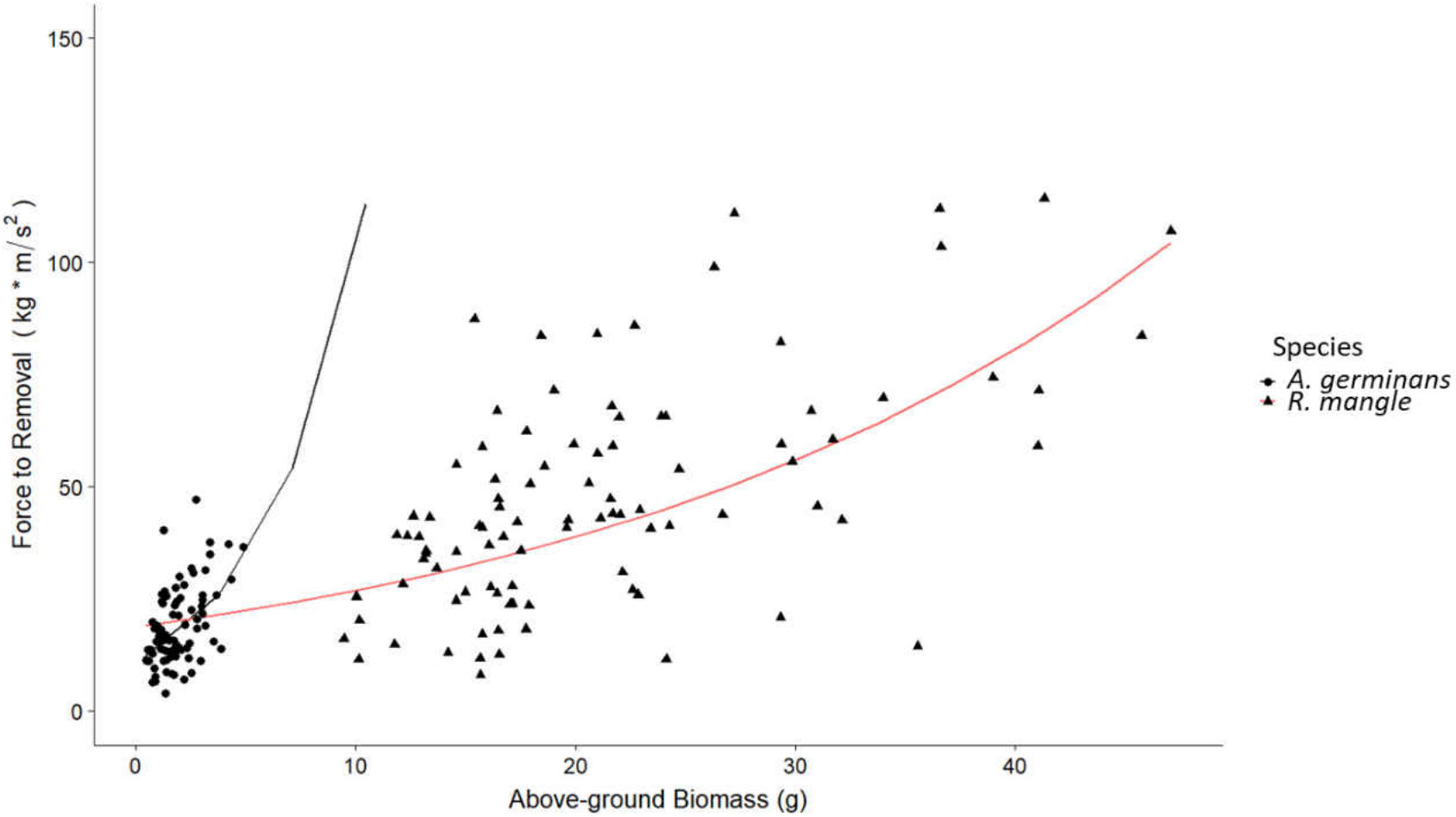

Figure 25: Model predictions for top performing model showing horizontal force to removal as a function of above-ground biomass and species for field pull-tests. Model predictions were made by simulating new above-ground biomass data to generate force to removal predictions for seedlings with equivalent biomass. The overlaid points represent the observed data.

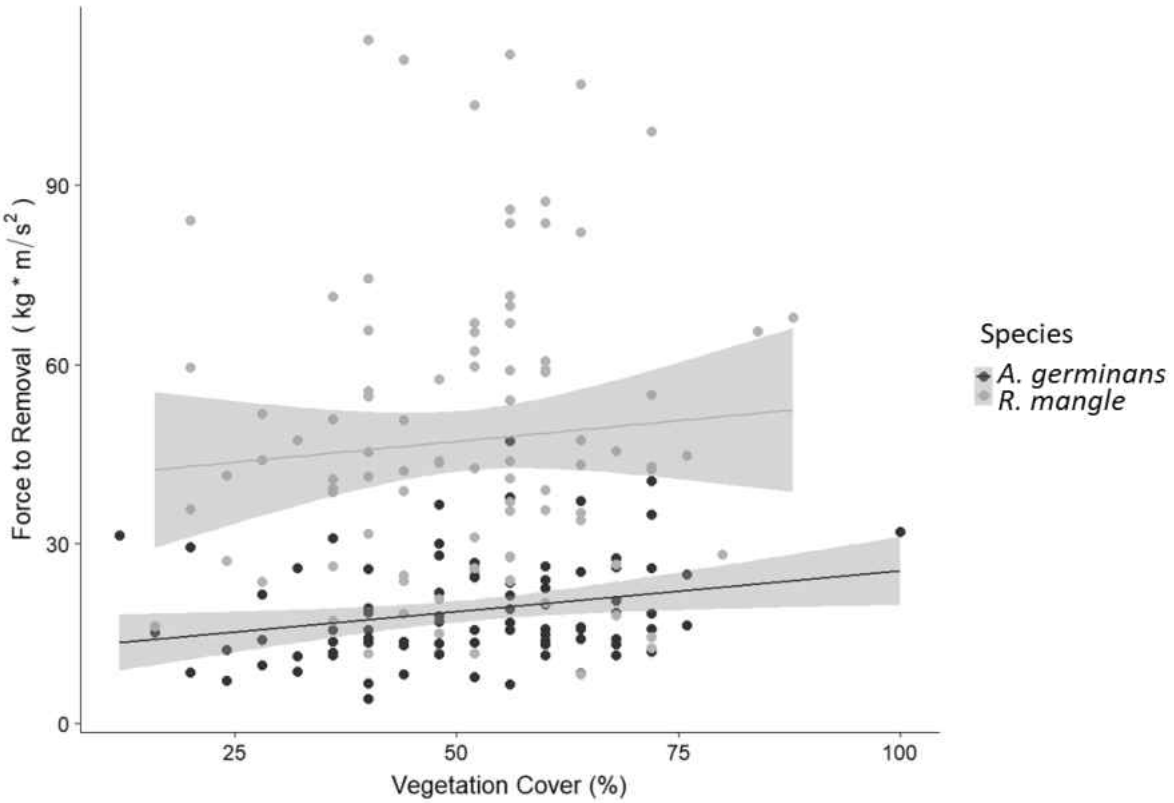

Figure 26: Force to removal as a function of vegetation cover (%) in surrounding 0.25 m^2.

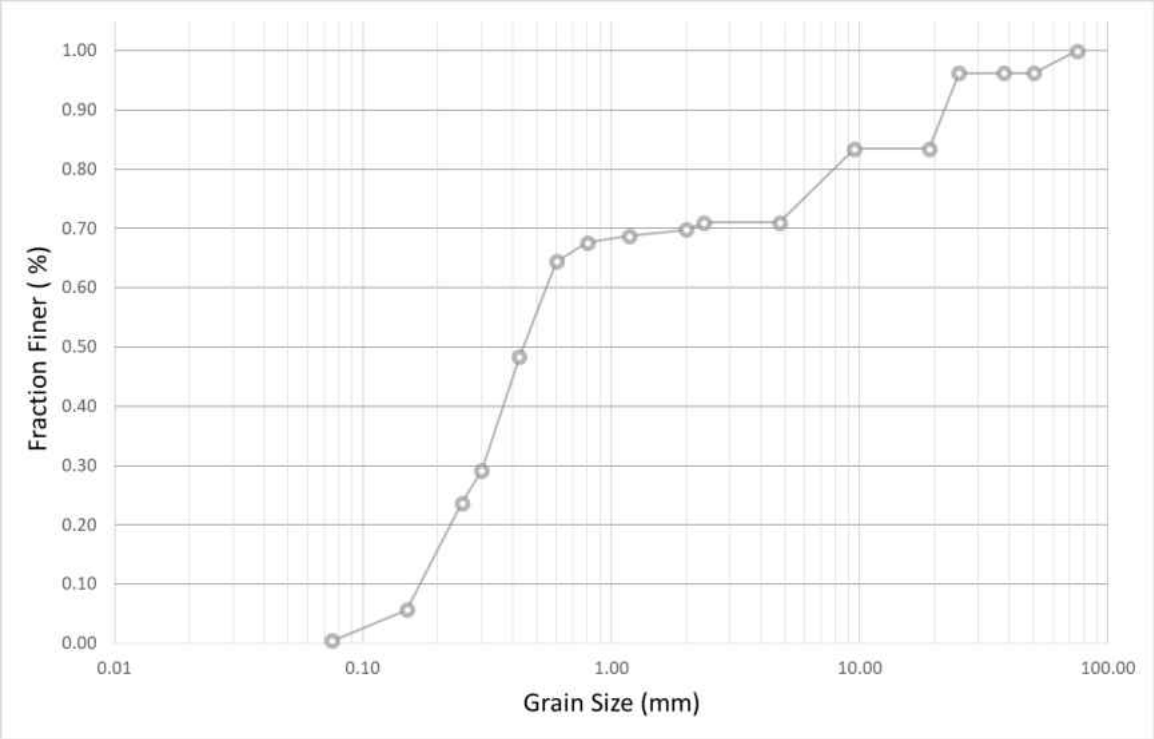

Figure 27: Average grain size distribution of the coarse sediment treatment used in greenhouse pull-tests on log scale. Values were measured using dry sieve analysis.

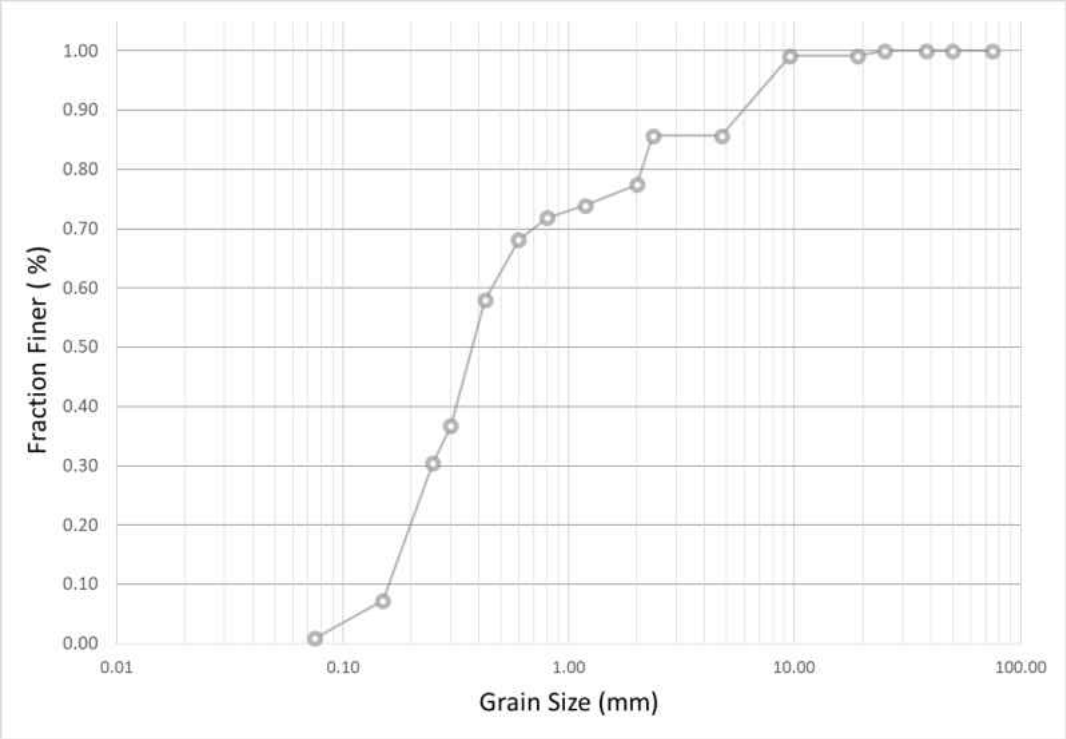

Figure 28: Average grain size distribution of the fine sediment treatment used in greenhouse pull-tests on log scale. Values were measured using dry sieve analysis.

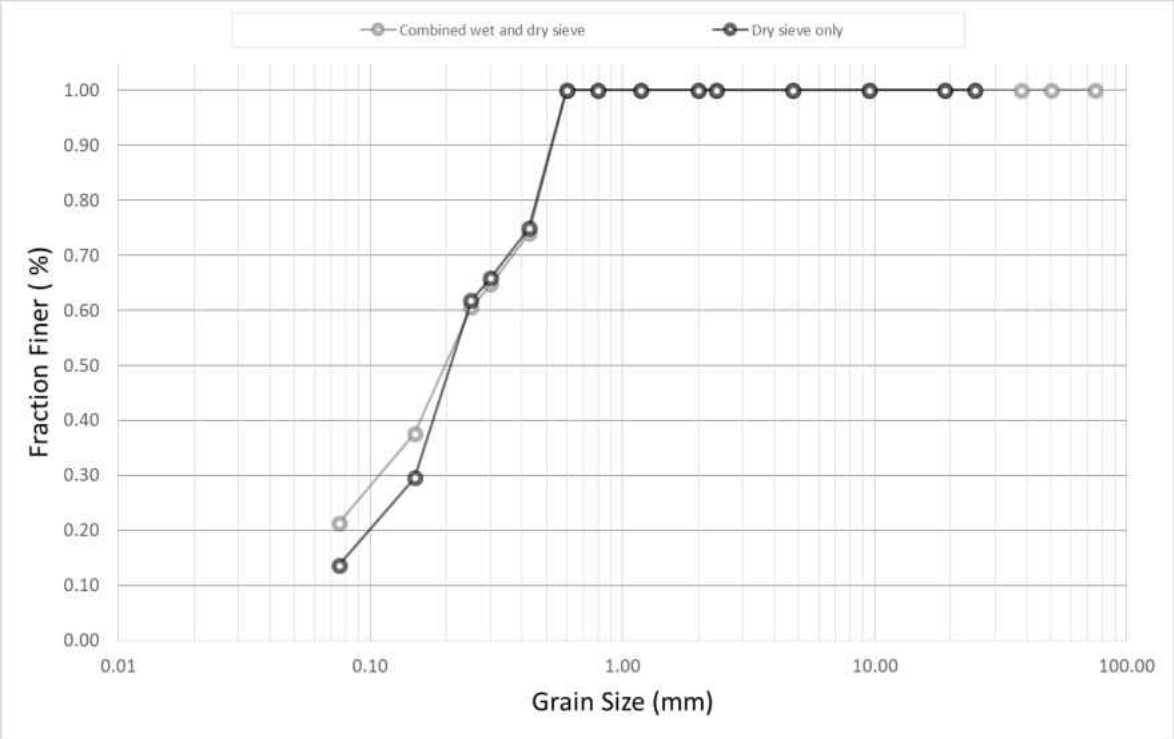

Figure 29: Average grain size distribution of sediment samples from Canaveral National Seashore field sites. Values were measured using dry sieve analysis and the combination of dry and wet sieve analysis.

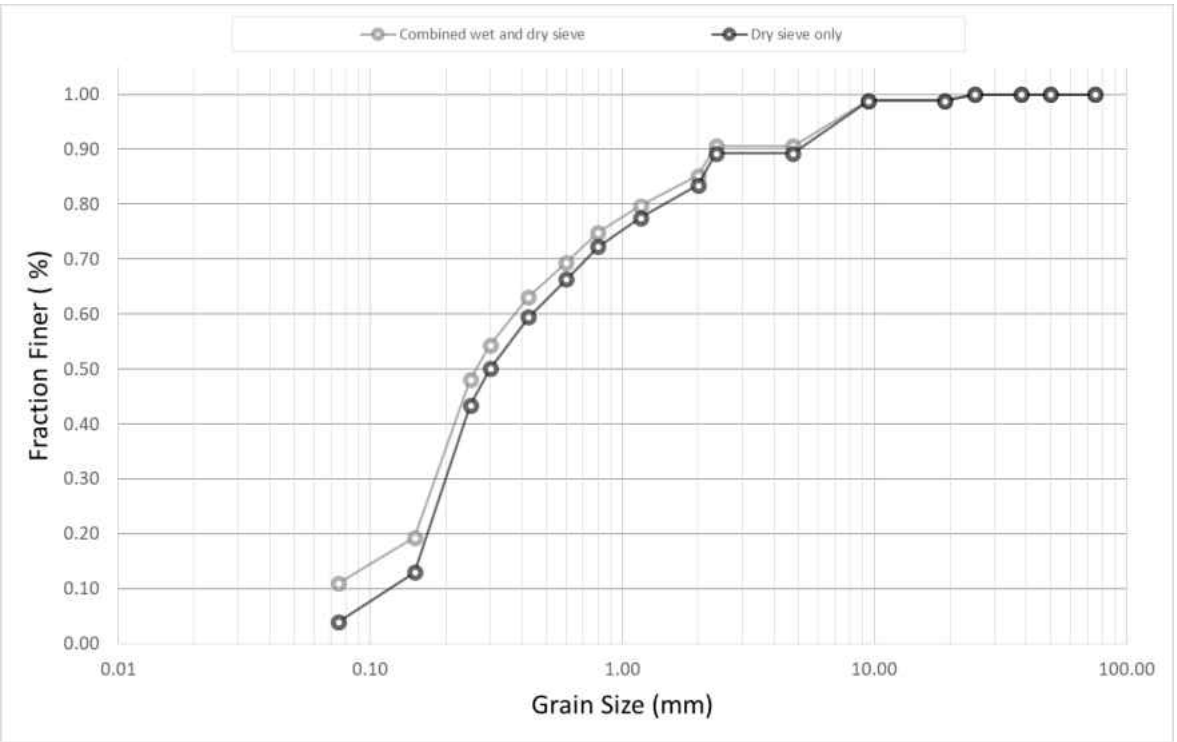

Figure 30: Average grain size distribution of sediment samples from De Soto National Memorial field sites. Values were measured using dry sieve analysis and the combination of dry and wet sieve analysis.

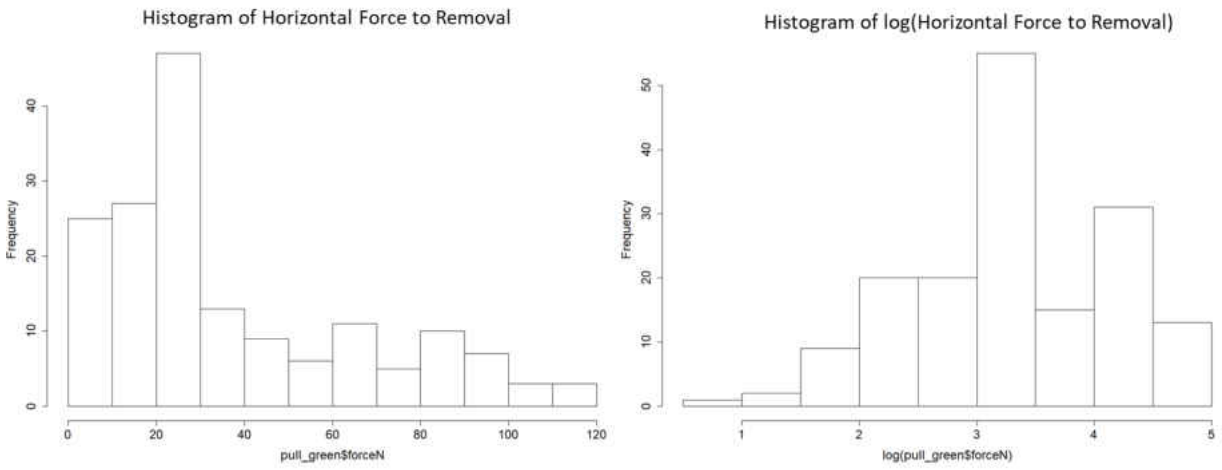

Figure 31: Histogram of horizontal force to removal and log(horizontal force to removal) for greenhouse pull-tests

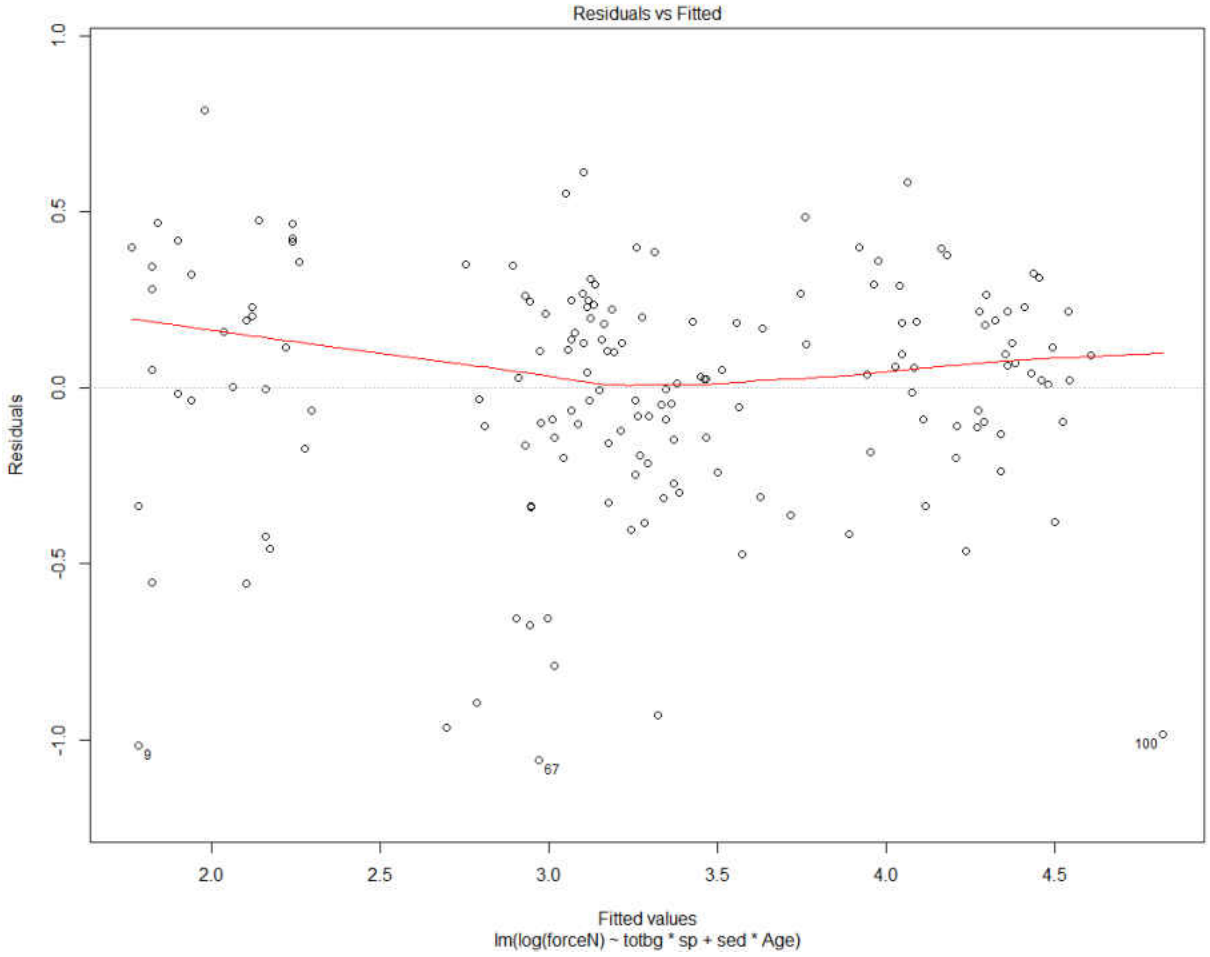

Figure 32: Residuals of model 9 predicting log transformed horizontal force to removal for greenhouse pull-tests.

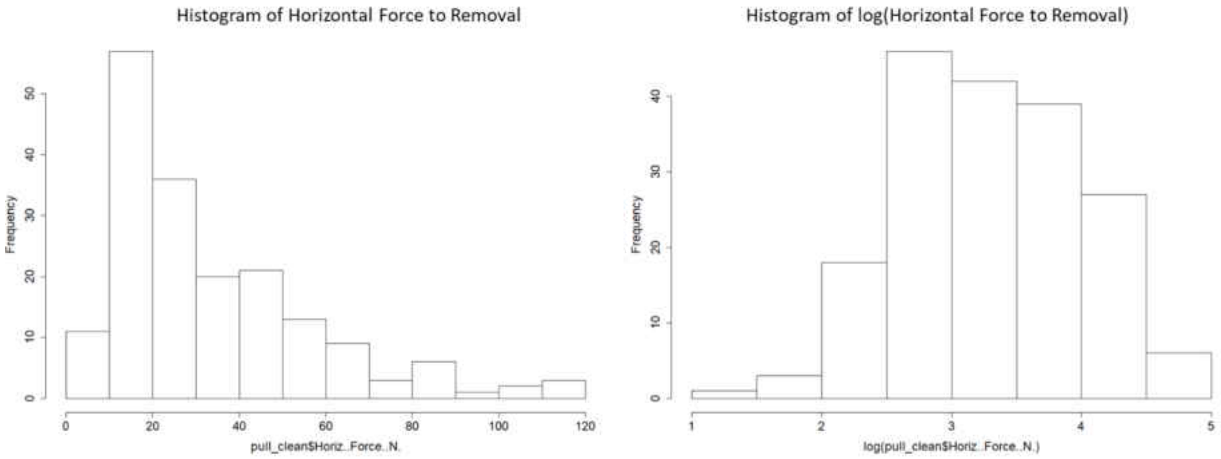

Figure 33: Histogram of horizontal force to removal and log(horizontal force to removal) for field pull-tests.

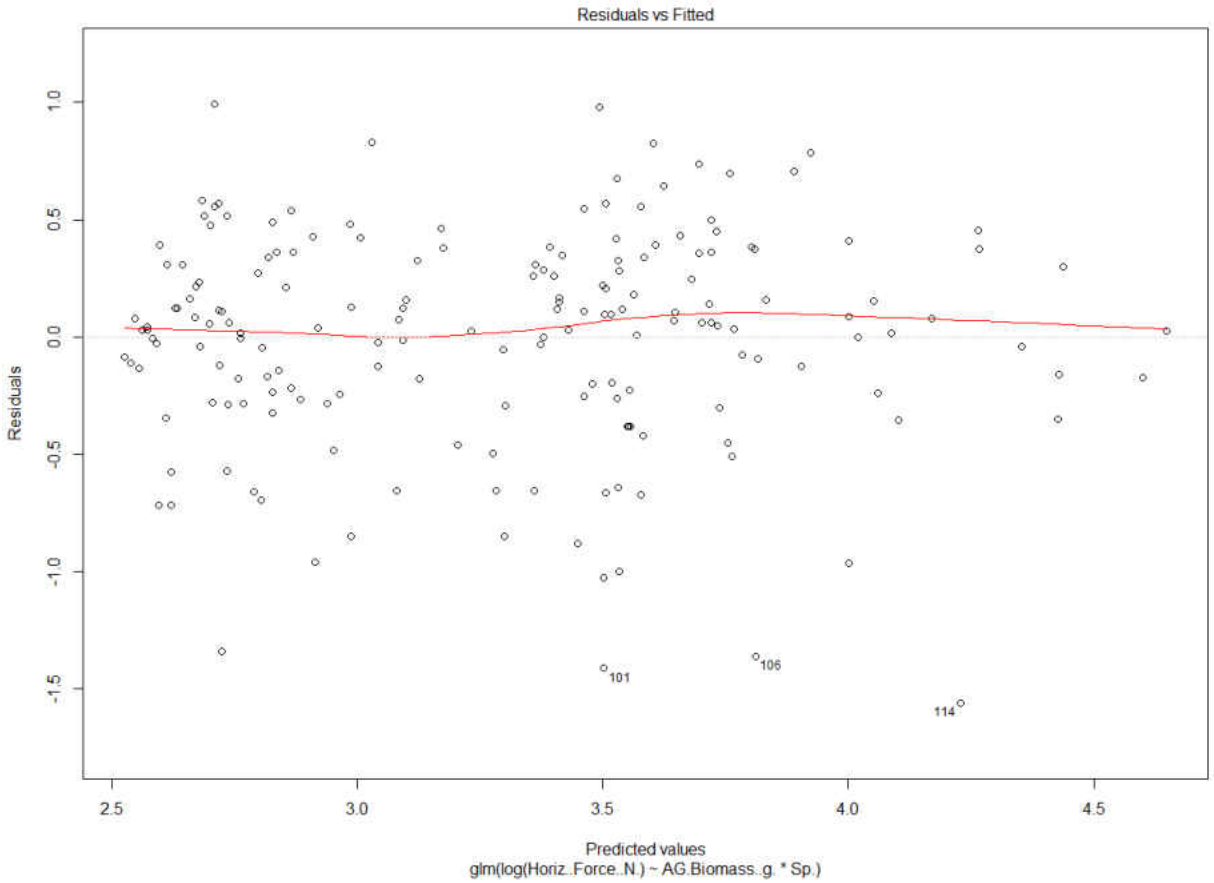

Figure 34: Residuals of model 4 predicting log transformed horizontal force to removal for field pull-tests.

Table 13: Mean propagule lengths (± S.E.) and percent of propagules rooting along shoreline transect surveys. Propagule statistics were calculated from the months with peak propagule abundance (August, September, and October) during the 2018 propagule season.

		August		September		October	
Shoreline Type	**Species**	**Length (cm)**	**Percent Rooting (%)**	**Length (cm)**	**Percent Rooting (%)**	**Length (cm)**	**Percent Rooting (%)**
Natural:	*R. mangle*	26.5 ± 1.4	5.0	16.0 ± 0.9	29.6	18.8 ± 2.1	66.7
	A. germinans	3.5 ± 0.1	25.4	4.3 ± 0.1	72.1	4.8 ± 0.2	62.2
	L. racemosa	2.5 ± 0.1	1.1	4.5 ± 0.3	39.4	3.9 ± 0.0	100
Restored:	*R. mangle*	17.3 ± 5.6	0.0	20.8 ± 3.5	62.5	13.7 ± 3.2	50.0
	A. germinans	2.3 ± 0.1	0.3	2.5 ± 0.0	3.4	4.4 ± 0.4	57.1
	L. racemosa	2 ± 0.0	0.0	2.9 ± 0.3	7.7	-	-
Revetment:	*R. mangle*	20.1 ± 4.0	0.0	-	-	23.5 ± 1.8	33.3
	A. germinans	4.2 ± 0.4	0.0	4.7 ± 0.2	0.0	8.0 ± 1.6	50.0
	L. racemosa	-	-	-	-	-	-

REFERENCES

Alongi, D.M., 2008. Mangrove forests: Resilience, protection from tsunamis, and responses to global climate change. Estuarine, Coastal and Shelf Science 76, 1–13. https://doi.org/10.1016/j.ecss.2007.08.024

Alongi, D. 2009. The Energetics of Mangrove Forests. Springer Science + Business Media B.V., Berlin, 216 pp.

Balke, T., Bouma, T.J., Horstman, E., Webb, E., Erftemeijer, P., Herman, P., 2011. Windows of opportunity: thresholds to mangrove seedling establishment on tidal flats. Marine Ecology Progress Series 440, 1–9. https://doi.org/10.3354/meps09364

Balke, T., Webb, E., Van den Elzen, E., Galli, D., Herman, P., Bouma, T.J, 2013. Seedlings establishment in a dynamic sedimentary environment: a conceptual framework using mangroves. Journal of Applied Ecology.50, 740-747. https://doi.org/10.1111/1365-2664.12067

Balke, T., Swales, A., Lovelock, C.E., Herman, P.M.J., Bouma, T.J., 2015. Limits to seaward expansion of mangroves: Translating physical disturbance mechanisms into seedling survival gradients. Journal of Experimental Marine Biology and Ecology 467, 16–25. https://doi.org/10.1016/j.jembe.2015.02.015

Ball, M., 1988. Ecophysiology of mangroves. Trees 2, 129-142. https://doi.org/10.1007/BF00196018

Barbier, E.B., Hacker, S.D., Kennedy, C., Koch, E.W., Stier, A.C., Silliman, B.R., 2011. The value of estuarine and coastal ecosystem services. Ecological monographs 81, 169–193.

Boizard, S.D., Mitchell, S.J., 2011. Resistance of red mangrove (Rhizophora mangle L.) seedlings to deflection and extraction. Trees 25, 371–381. https://doi.org/10.1007/s00468-010-0512-z

Bolker, B., and R Development Core Team. 2017. bbmle: Tools for General Maximum Likelihood Estimation. R package version 1.0.20. https://CRAN.R-project.org/package=bbmle

Bosire, J.O., Dahdouh-Guebas, F., Walton, M., Crona, B.I., Lewis, R.R., Field, C., Kairo, J.G., Koedam, N., 2008. Functionality of restored mangroves: A review. Aquatic Botany 89, 251–259. https://doi.org/10.1016/j.aquabot.2008.03.010

Bouma, T.J., Vries, M.B.D., Low, E., Kusters, L., Herman, P.M.J., Tánczos, I.C., Temmerman, S., Hesselink, A., Meire, P., Van Regenmortel, S., 2005. Flow hydrodynamics on a mudflat and in salt marsh vegetation: identifying general relationships for habitat characterisations. Hydrobiologia 540, 259–274. https://doi.org/10.1007/s10750-004-7149-0

Bywater-Reyes, S., Wilcox, A.C., Stella, J.C., Lightbody, A.F., 2015. Flow and scour constraints on uprooting of pioneer woody seedlings: CONSTRAINTS ON UPROOTING OF SEEDLINGS. Water Resources Research 51, 9190–9206. https://doi.org/10.1002/2014WR016641

Campbell, D. 2015. Quantifying the effects of boat wakes on intertidal oyster reefs in a shallow estuary. M.S. thesis. University of Central Florida.

Carlos, C., Delfino, R.J., Juanico, D.E., David, L., Lasco, R., 2015. Vegetation resistance and regeneration potential of *Rhizophora, Sonneratia* and *Avicennia* in the Typhoon Haiyan-

affected mangroves in the Philippines: Implications on rehabilitation practices. Climate, Disaster and Development Journal 1, 1–8. https://doi.org/10.18783/cddj.v001.i01.a01

Caratti, J. F. 2006. Point Intercept (PO). USDA Forest Service. General Technical Report RMRS-GTR-164-CD, 17 pp.

Cavanaugh, K., Kellner, J., Forde, A., Gruner, D., Parker, J., Rodriguez, W., Feller, I., 2013. Poleward expansion of mangroves is a threshold response to decreased frequency of extreme cold events. Proceedings of the National Academy of Sciences. 111, 723-727. https://doi.org/10.1073/pnas.1315800111

Delgado, P., Hensel, P., Jiménez, J.., Day, J.., 2001. The importance of propagule establishment and physical factors in mangrove distributional patterns in a Costa Rican estuary. Aquatic Botany 71, 157–178. https://doi.org/10.1016/S0304-3770(01)00188-7

Di Nitto, D., Dahdouh-Guebas, F., Kairo, J., Decleir, H., Koedam, N., 2008. Digital terrain modelling to investigate the effects of sea level rise on mangrove propagule establishment. Marine Ecology Progress Series 356, 175–188. https://doi.org/10.3354/meps07228

Donnelly, M., Shaffer, M., Connor, S., Sacks, P., Walters, L. J., 2017. Using mangroves to stabilize coastal historic sites: deployment success versus natural recruitment. Hydrobiologia 803, 389–401. https://doi.org/10.1007/s10750-017-3155-x

Donnelly, M.J., Walters, L.J., 2008. Water and Boating Activity as Dispersal Vectors for *Schinus terebinthifolius* (Brazilian pepper) Seeds in Freshwater and Estuarine Habitats. Estuaries and Coasts 31, 960–968. https://doi.org/10.1007/s12237-008-9092-1

Duarte, C., Geertz-Hansen, O., Thampanya, U., Terrados, J., Fortes, M., Kamp-Nielsen, L., Borum, J., Boromthanarath, S., 1998. Relationship between sediment conditions and mangrove *Rhizophora apiculata* seedling growth and nutrient status. Marine Ecology Progress Series 175, 277–283. https://doi.org/10.3354/meps175277

Ellison, A.M., Farnsworth, E.J., Seedling Survivorship, Growth, and Response to Disturbance in Belizean Mangal. American Journal of Botany 10, 1137-1145.

Feller, I.C., Friess, D.A., Krauss, K.W., Lewis, R.R., 2017. The state of the world's mangroves in the 21st century under climate change. Hydrobiologia 803, 1–12. https://doi.org/10.1007/s10750-017-3331-z

Feller, I.C., Lovelock, C.E., McKee, K.L., 2007. Nutrient Addition Differentially Affects Ecological Processes of *Avicennia germinans* in Nitrogen versus Phosphorus Limited Mangrove Ecosystems. Ecosystems 10, 347–359. https://doi.org/10.1007/s10021-007-9025-z

Food and Agriculture Organization (FAO), 2007. The World's Mangroves 1980–2005, FAO Forestry Paper 153

Friess, D.A., Krauss, K.W., Horstman, E.M., Balke, T., Bouma, T.J., Galli, D., Webb, E.L., 2012. Are all intertidal wetlands naturally created equal? Bottlenecks, thresholds and knowledge gaps to mangrove and saltmarsh ecosystems. Biological Reviews 87, 346–366. https://doi.org/10.1111/j.1469-185X.2011.00198.x

Fritz, H.M., Borrero, J.C., Synolakis, C.E., Yoo, J., 2006. 2004 Indian Ocean tsunami flow velocity measurements from survivor videos. Geophysical Research Letters 33. https://doi.org/10.1029/2006GL026784

Garel, E., López Fernández, L., Collins, M., 2008. Sediment resuspension events induced by the wake wash of deep-draft vessels. Geo-Marine Letters 28, 205–211. https://doi.org/10.1007/s00367-008-0101-y

Gedan, K.B., Kirwan, M.L., Wolanski, E., Barbier, E.B., Silliman, B.R., 2011. The present and future role of coastal wetland vegetation in protecting shorelines: answering recent challenges to the paradigm. Climatic Change 106, 7–29. https://doi.org/10.1007/s10584-010-0003-7

Giri, C., Ochieng, E., Tieszen, L.L., Zhu, Z., Singh, A., Loveland, T., Masek, J., Duke, N., 2011. Status and distribution of mangrove forests of the world using earth observation satellite data. Global Ecology and Biogeography 20, 154–159.

Gittman, R.K., Peterson, C.H., Currin, C.A., Joel Fodrie, F., Piehler, M.F., Bruno, J.F., 2016. Living shorelines can enhance the nursery role of threatened estuarine habitats. Ecological Applications 26, 249–263. https://doi.org/10.1890/14-0716

Hartig, F. 2019. DHARMa: Residual Diagnostics for Hierarchical (Multi-Level / Mixed) Regression Models. R package version 0.2.2. https://CRAN.R-project.org/package=DHARMa

Hlavac, M. 2018. Stargazer: Well-Formatted Regression and Summary Statistics Tables. R package version 5.2.1. https://CRAN.R-project.org/package=stargazer

Horstman, E., Dohmen-Janssen, M., Narra, P., Van den Berg, N.-J., Siemerink, M., Balke, T., Bouma, T., Hulscher, S., 2012. Wave attenuation in mangrove forests; field data obtained

in Trang, Thailand. Coastal Engineering Proceedings 1, 40. https://doi.org/10.9753/icce.v33.waves.40

Houser, C., 2010. Relative Importance of Vessel-Generated and Wind Waves to Salt Marsh Erosion in a Restricted Fetch Environment. Journal of Coastal Research 262, 230–240. https://doi.org/10.2112/08-1084.1

Kamali, B., Hashim, R., 2011. Mangrove restoration without planting. Ecological Engineering 37, 387–391. https://doi.org/10.1016/j.ecoleng.2010.11.025

Kathiresan, K., 2003. How do mangrove forests induce sedimentation? Revista de Biologia Tropical. 51, 355-360

Kathiresan, K., Qasim, S. Z., 2005. Biodiversity of Mangrove Ecosystems. Hindustan Publishing Corporation, India, 251 pp.

Kibler, K. M., Kitskoudis, V., Donnelly, M., Spiering, D. W., Walters, L. J., Flow-biota interaction in coastal restoration: hydrodynamics influence mangrove recruitment success in restored shorelines. *Sustainability,* in review.

Krauss, K.W., Lovelock, C.E., McKee, K.L., López-Hoffman, L., Ewe, S.M.L., Sousa, W.P., 2008. Environmental drivers in mangrove establishment and early development: A review. Aquatic Botany 89, 105–127. https://doi.org/10.1016/j.aquabot.2007.12.014

Le Minor, M., Bartzke, G., Zimmer, M., Gillis, L., Helfer, V., Huhn, K., 2019. Numerical modelling of hydraulics and sediment dynamics around mangrove seedlings: Implications for mangrove establishment and reforestation. Estuarine, Coastal and Shelf Science 217, 81–95. https://doi.org/10.1016/j.ecss.2018.10.019

Lewis, R.R., 2000. Ecologically based goal setting in mangrove forest and tidal marsh restoration. Ecological Engineering 15, 191–198. https://doi.org/10.1016/S0925-8574(00)00070-7

Lewis, R.R., 2005. Ecological engineering for successful management and restoration of mangrove forests. Ecological Engineering 24, 403–418. https://doi.org/10.1016/j.ecoleng.2004.10.003

Lightbody, A. F., Nepf, H.M., 2006. Prediction of velocity profiles and longitudinal dispersion in emergent salt marsh vegetation, Limnology and Oceanography 51, 218–228. https://doi-org.ezproxy.net.ucf.edu/10.4319/lo.2006.51.1.0218

Lima, K.O. de O., Tognella, M.M.P., Cunha, S.R., Andrade, H.A. de, 2018. Growth models of Rhizophora mangle L. seedlings in tropical southwestern Atlantic. Estuarine, Coastal and Shelf Science 207, 154–163. https://doi.org/10.1016/j.ecss.2018.03.021

Liu, C., Evett, J. 2008. Soil Properties: Testing, Measurement, and Evaluation (6th Edition). Pearson, United Kingdom, 448 pp.

Mazda, Y., Kobashi, D., Okada, S., 2005. Tidal-Scale Hydrodynamics within Mangrove Swamps. Wetlands Ecology and Management 13, 647–655. https://doi.org/10.1007/s11273-005-0613-4

Mazda, Y., Wolanski, E., King, B., Sase, A., Ohtsuka, D., Magi, M., 1997. Drag force due to vegetation in mangrove swamps. Mangroves and Salt Marshes 1, 193-199.

McKee, K.L., 1995. Interspecific Variation in Growth, Biomass Partitioning, and Defensive Characteristics of Neotropical Mangrove Seedlings – Response to Light and Nutrient Availability. American Journal of Botany. 82, 299-307. https://doi.org/10.2307/2445575

Minchinton, T.E., 2001. Canopy and substratum heterogeneity influence recruitment of the mangrove Avicennia marina. Journal of Ecology 89, 888-902.

Mullarney, J.C., Henderson, S.M., Reyns, J.A.H., Norris, B.K., Bryan, K.R., 2017. Spatially varying drag within a wave-exposed mangrove forest and on the adjacent tidal flat. Continental Shelf Research 147, 102–113. https://doi.org/10.1016/j.csr.2017.06.019

Mullarney, J.C., Henderson, S.M., 2017. Flows within marine vegetation canopies. In: Kaihatu, J., Panchang, V. (Eds.), Advances in Coastal Hydraulics World. Scientific Publishing Ltd., Singapore, pp. 1-46

National Park Service. 2019. De Soto National Memorial. URL: https://www.nps.gov/deso/index.htm. Accessed March 31, 20190.

Odum, W.E., McIvor, C.C., Smith III, T.J., 1982. The ecology of the mangroves of south Florida: a community profile. U.S. Fish and Wildlife Service, Office of Biological Services, Washington, D.C. FWS/OBS-81/24. 144 pp.

Pasquale, N., Perona, P., Francis, R., Burlando, P., 2014. Above-ground and below-ground *Salix* dynamics in response to river processes. Hydrological Processes 28, 5189–5203. https://doi-org.ezproxy.net.ucf.edu/10.1002/hyp.9993

Polidoro, B.A., Carpenter, K.E., Collins, L., Duke, N.C., Ellison, A.M., Ellison, J.C., Farnsworth, E.J., Fernando, E.S., Kathiresan, K., Koedam, N.E., Livingstone, S.R., Miyagi, T., Moore, G.E., Ngoc Nam, V., Ong, J.E., Primavera, J.H., Salmo, S.G., Sanciangco, J.C., Sukardjo, S., Wang, Y., Yong, J.W.H., 2010. The Loss of Species: Mangrove Extinction Risk and Geographic Areas of Global Concern. PLoS ONE 5, e10095. https://doi.org/10.1371/journal.pone.0010095

Poorter, H., Nagel, O., 2000. The role of biomass allocation in the growth response of plants to different levels of light, CO2, nutrients and water: a quantitative review. Functional Plant Biology 27, 1191. https://doi.org/10.1071/PP99173_CO

R Core Team. 2018. R: A language and environment for statistical computing. R Foundation for Statistical Computing, Vienna, Austria. https://www.R-project.org/.

Rapaglia, J., Zaggia, L., Ricklefs, K., Gelinas, M., Bokuniewicz, H., 2011. Characteristics of ships' depression waves and associated sediment resuspension in Venice Lagoon, Italy. Journal of Marine Systems 85, 45–56. https://doi.org/10.1016/j.jmarsys.2010.11.005

Robert, E.M.R., Oste, J., Van der Stocken, T., De Ryck, D.J.R., Quisthoudt, K., Kairo, J.G., Dahdouh-Guebas, F., Koedam, N., Schmitz, N., 2015. Viviparous mangrove propagules of Ceriops tagal and Rhizophora mucronata, where both Rhizophoraceae show different dispersal and establishment strategies. Journal of Experimental Marine Biology and Ecology 468, 45–54. https://doi.org/10.1016/j.jembe.2015.03.014

Shan, Y., Liu, C., Nepf, H., 2019. Comparison of drag and velocity in model mangrove forests with random and in-line tree distributions. Journal of Hydrology 568, 735–746. https://doi.org/10.1016/j.jhydrol.2018.10.077

Sheremet, A., Gravois, U., Tian, M., 2013. Boat-Wake statistics at Jensen Beach, Florida. Journal of Waterway, Port, Coastal, and Ocean Engineering 139, 286–294. https://doi.org/10.1061/(ASCE)WW.1943-5460.0000182

Simpson, L.T., Osborne, T.Z., Feller, I.C., 2017. Establishment and Biomass Allocation of Black and Red Mangroves: Response to Propagule Flotation Duration and Seedling Light

Availability. Journal of Coastal Research 335, 1126–1134. https://doi.org/10.2112/JCOASTRES-D-16-00108.1

Sousa, W.P., Kennedy, P.G., Mitchell, B.J., Ordóñez L, B.M., 2007. Supply-side Ecology in Mangroves: Do propagule dispersal and seedling establishment explain forest structure? Ecological Monographs 77, 53–76. https://doi.org/10.1890/05-1935

Spiering, D.W., Kibler, K. M., Kitskoudis, V., Walters, L. J., Hydrodynamic changes following a living shoreline restoration based upon a Before-After-Control-Impact design. *Estuaries and Coasts*, in review.

Struve, J., Falconer, R.A., Wu, Y., 2003. Influence of model mangrove trees on the hydrodynamics in a flume. Estuarine, Coastal and Shelf Science 58, 163–171. https://doi.org/10.1016/S0272-7714(03)00072-6

Wickham, H., 2009. Ggplot2: Elegant Graphics for Data Analysis. Springer-Verlag New York. ISBN 978-0-387-98140-6, <URL: http://ggplot2.org>.

Wolanski, E., Mazda, Y., King, B., Gay, S., 1990. Dynamics, flushing and trapping in Hinchinbrook channel, a giant mangrove swamp. Australia. Estuarine, Coastal and Shelf Science 31, 55-579

Van der Stocken, T., Carroll, D., Menemenlis, D., Simard, M., Koedam, N., 2019. Global-scale dispersal and connectivity in mangroves. Proceedings of the National Academy of Sciences 116, 915-922. https://doi.org/10.1073/pnas.1812470116

Zhang, X., Chua, V.P., Cheong, H.-F., 2015. Hydrodynamics in mangrove prop roots and their physical properties. Journal of Hydro-environment Research 9, 281–294. https://doi.org/10.1016/j.jher.2014.07.010